The influence of the two-component grout on the behaviour of a segmental lining in tunnelling

The influence of the two-component grout on the behaviour of a segmental lining in tunnelling

Claudio Oggeri[1], Pierpaolo Oreste[2], Giovanni Spagnoli[3]

[1] Department of Environment, Land and Infrastructure Engineering, Politecnico di Torino, Corso Duca Degli Abruzzi 24, 10129 Torino, Italy, *claudio.oggeri@polito.it* ORCID 0000-0002-6848-8861

[2] Department of Environment, Land and Infrastructure Engineering, Politecnico di Torino, Corso Duca Degli Abruzzi 24, 10129 Torino, Italy, *pierpaolo.oreste@polito.it* ORCID: 0000-0001-8227-9807

[3] MBCC Group, Dr-Albert-Frank-Strasse 32, 83308 Trostberg, Germany, Tel: +49 8621 86-3702, *giovanni.spagnoli@mbcc-group.com* ORCID: 0000-0002-1866-4345

Abstract

Filling material is present around the segment lining when a shielded Tunnel Boring Machine is used to excavate a tunnel. The two-component grout is becoming lately one of the most used filling materials. Its mechanical properties evolve over time. Unfortunately, there are not many studies in the literature on the specific mechanical characteristics of these materials. This work presents the results obtained from an extensive laboratory test campaign that allowed to fully characterize the two-component filling material during the setting period. In particular, the values of the stiffness and resistance parameters were obtained over time, where uniaxial compression tests and oedometer tests were carried out. A detailed study of the effect of the presence of the filling material on the behavior of the support system (segmental lining + filling material) was developed for two of the most widespread analytical methods for the analysis of the behavior of tunnels and structures of

support: the convergence-confinement method and the Einstein and Schwartz method. Subsequent parametric analyses made it possible to consider the variability of the influencing parameters within the typical variability ranges obtained from the laboratory test campaign or known from the available scientific literature. From the study carried out, it was possible to note that it is necessary to consider the presence of the filling material in the evaluation of the stiffness of the support system, when using the convergence-confinement method to estimate the loads acting on segmental lining. In this regard, it is necessary to have a reliable estimate of the elastic modulus of the filling material in the period of loading of the segmental lining. On the other hand, the presence of the ring of filling material is negligible when evaluating the state of stress of the segmental lining with specific methods capable of considering the rock-support interaction. In particular, adopting the Einstein and Schwartz method, it is possible to define the bending moments and normal forces acting in the support structure, referring to the stiffness parameters of the segmental lining alone.

Key words: two-component grout; curing time; oedometer; unconfined compressive strength; TBM; convergence-confinement method; Einstein and Schwartz method.

Abbreviations and nomenclature

A_s Area of the cross section of the support, through a plane passing through the axis of the tunnel;

b_s Width of the support section in the direction of the tunnel axis, considered equal to 1 m;

c Cohesion of the rock mass;

C^* Compressibility ratio of the support;

E Elastic modulus of the rock mass

E_{fm} Elastic modulus of the filling material;

$E_{s,eq}$ Equivalent elastic modulus of the support;

E_{sl} Elastic modulus of the segmental lining concrete;

F^* Flexibility ratio of the support;

I_s Moment of inertia of the cross section of the support, through a plane passing through the axis of the tunnel;

K_0 Lateral earth coefficient at rest;

k_{sys} Reaction line of the support the stiffness;

M_{max} Maximum bending moment present in the lining;

N Normal force present in the lining;

p Pressure inside the tunnel acting on the walls;

p_{eq} Final entity of the loads acting on the support structure;

p_0 Hydrostatic initial stress state (undisturbed);

R Tunnel radius;

R_{pl} Plastic radius of the tunnel;

$t_{s,eq}$ Thickness of equivalent support;

t_{fm} Thickness of the filling material;

t_{sl} Thickness of the segmental lining;

u_{eq} Final displacement of the tunnel wall in the radial direction;

u_{max} Maximum displacement of the tunnel wall in the absence of supports;

u_0 Displacement of the tunnel wall when the support structure is installed;

u_R Radial displacement of the tunnel wall;

ν Poisson ratio of the rock mass;

ν_{fm} Poisson's ratio of the filling material;

ν_{sl} Poisson's ratio of the concrete constituting the segmental lining;

α_f Angle of the failure plane;

φ Friction angle of the rock mass;

Ψ Dilatancy of the rock mass;

σ_r Radial stress in the point where the stress state is evaluated during the desgin of the support structure;

σ_{vert} or σ_v Vertical load during the oedometer tests;

$\sigma_{\vartheta,sl,in}$ Circumferential stress at the intrados of the segmental lining due to moment;

$\sigma_{\vartheta,fm,ex}$ Maximum circumferential load on the extrados of the filling material due to the moment;

$\sigma_{\vartheta,sl}$ Constant load in the segmental lining section due to the nominal force;

$\sigma_{\vartheta,fm}$ Constant load in the section of the filling material due to the nominal force;

ξ Incremental coefficient taking into into account the transfer of stresses from one ring to the adjacent one, in correspondence with the longitudinal joints of the segmental lining;

η Reduction coefficient taking into account the presence of longitudinal joints in segmental lining;

ϕ' Slope the Mohr Coulomb envelope.

1. Introduction

During the excavation with shielded tunnel boring machines (S-TBM) pre-cast segments are commonly installed as tunnel lining and for support purpose. Due to overcutting of the circular tunnel profile due to the TBM cutterhead excavation, a circular gap between the lining and the surrounding ground is formed (thickness about 13 to 20 cm, e.g. Talmon and Bezuijen, 2005; Beghoul and Demagh, 2019). This space must be filled by pumping or injecting some materials, such as the so-called “annulus grout” (Fig. 1). The practical aims for the use of the filler are linked to control the ground deformation around the lining gap and the reduction of the ground loss; there is also a role to contribute in a regular and homogeneous distribution of the contact pressure at the interfaces ground/grout and grout/segmental lining.

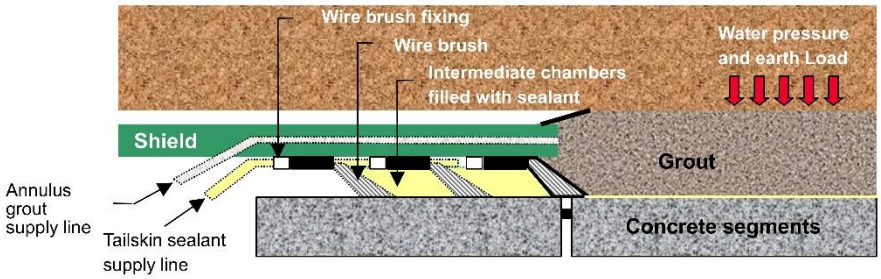

Fig. 1. Sketch of the annulus grout.

There are two basic types of annular grouts currently in use: thick mortar type grouts and highly mobile two-component grouts. The typical mix-design in a m^3 system for a two-component grout is very variable and depends strongly on the project specification but in general it consists of cement (280-450 kg), bentonite (30-60 kg), water (730-860 kg), retarder 3-5 kg) and accelerator, normally sodium silicate (60-80 kg).

The accelerator (“B” component) is generally added just before pumping phase of the mix of water, bentonite, retarder and cement (“A” component).

The excavation of the tunnel produces a relaxation of the initial tensional state, leading to deformations in the ground from certain distance ahead of the excavation face. The convergence in the tunnel is the inward displacements of the soil/rock as consequence of the relief of the initial stress. In case of no support, the ground is free to deform into the cavity until arriving to the equilibrium state.

The role of the two-component grout is very important for the correct mechanized tunneling procedure in order to minimize surface settlements due to any over-excavation generated by the passage of the TBM (e.g. Maidl et al., 1995) or to minimize the loads acting on the segmental lining, although grouting can also be used for the same aims (e.g. Komiya et al., 2001). The two-component grout should be water-tight, be pumpable, be workable, able to fill the void, not able to shrink, to stiff quickly and to be wash-out resistant (e.g. Thewes and Budach, 2009). Its mechanical strength, though, should be only slightly higher than that of the surrounding soil to prevent substantial normal force components being removed from the annular gap mortar in the final state (DAUB, 2013). Simultaneous backfilling with two-component grouts, in comparison with the mortar type grouts, keeps in general lower settlements during TBM excavation (Hirata, 1989) and normally the lining pressures, few rings behind the TBM, do not change significantly in the long-term (Hashimoto et al., 2004).

However, not many works dealt with the behavior of the two-component grouts both experimentally and numerically (e.g. Pelizza et al., 2011; Shah et al., 2018; Ochmański et al., 2018; Todaro et al., 2019). For instance, it is well-known that the mechanical properties of the two-component grout change based on the mix-design type (Flores, 2015; Todaro et al., 2019). Besides, tail void grouting, as it cannot be directly observed after the tunnel construction, is difficult to simulate (Dai et al., 2010). Oh and Ziegler (2014), Shah et al. (2018), Ochmański et al. (2018) more recently Ochmański et al. (2020) performed a

numerical analysis regarding the effects of the two-component grout on the tunnel settlement. Bezuijen and Talmon (2003) and Dias and Bezuijen (2015) investigated the consolidation of the grout, which seems to be dependent on the permeability of the surrounding soil as the latter determines the rate of outflow. Therefore, a very impermeable soil like a clay could stop the grout from consolidating (Vu et al. 2016), however in permeable soils, fluid loss occurs during grout consolidation (Talmon and Bezuijen, 2005). Furthermore, Bezuijen and Talmon (2003) and Dias and Bezuijen (2015) illustrate that during this consolidation, the grout mixture becomes thicker (the cement-water ratio increases, decreasing the viscosity of the mixture). Talmon and Bezuijen (2005) investigated the stress-strain modelling of the grout.

However, the role of the material considering the deformability and resistance values that characterize it during the loading phase of the segmental lining tunnel are not fully investigated. The two-component grout when hardens should transmit the tunnel deformation to the ground. In literature, ground settlement in tunneling caused by ground loss (i.e. the difference between actual and theoretical excavation volume) considers also tail loss which occurs along the annular void between ground and concrete segmental lining (as a result of shrinkage or compression of backfill grout material).The gap model proposed by Lee et al. (1992) is based on simple elastic equations for the squeezing of tunnel face and the contraction of excavated cavity and it has some limitations and uncertainties for practical use (Park et al., 2018). Finally, features of specific products and fulfillment of requirements should be addressed when adopting design criteria and accepting construction procedures: materials, environmental requirements and use of chemicals products should be approved by Client and Boards for a reliable practical quality assurance (Oggeri and Ova, 2004). Furthermore, the use of numerical modeling in tunneling, both with two-dimensional and three-dimensional methods, requires the definition of the characteristics of all the materials that are used as support structures or

rock reinforcement interventions (Do et al., 2014a; 2014b; 2015; 2016; Pelizza et al., 2000).

In this paper, a mix-design of a two-component grout was analyzed in the detail. Unconfined compressive strength (UCS) and oedometer tests at varying curing ages were investigated. From the analysis of the laboratory results it was possible to detect the behavior of this material and in particular the deformability and strength values that characterize it during the loading phase of the segmental lining tunnel.

Two very interesting simplified approaches are available in the literature to study the behavior of the supporting structures in tunnelling: the convergence-confinement method (e.g. Oreste, 2007; Oreste et al., 2016; 2018a; 2018b; Spagnoli et al., 2016; 2017) and the method of Einstein and Schwartz (1979). The convergence-confinement method considers the ground response to the advancing tunnel face and the interaction with installed support (e.g. Oke et al. 2018), whereas the latter method assumes an annular support continuously connected with the wall of a deep and circular tunnel.

This article describes the techniques for correctly considering the presence of the filling material in the gap between the tunnel segmental lining and the tunnel wall using the two widespread simplified analysis methods listed above. Some calculation examples will allow to evaluate the effect of the filling material on the static behavior of the tunnel segmental lining, starting from the mechanical parameters evaluated by the extensive laboratory testing campaign. From the developed analyses it will be possible to obtain useful information on how to consider the presence of the filling material ring in the design phase of the segmental lining of a tunnel.

2. The mechanical behavior of the two-component grout in the laboratory

Testing procedures

The following mix-design was tested during this experimental campaign: water 800 g, bentonite 35 g, cement (CEM I 52.5) 350 g, retarder 17.5 g (solution contains 20% solid therefore retarder dosage by weight of cement is 1%) and water glass (sodium silicate) 85 g (water glass is the “B” component so it is about 7% weight of the mix represented by the component “A”). Based on the grout component quantities, a preliminary laboratory testing set has been carried out. The purpose of such a trial was to identify the basic mechanical properties of the grout at different duration of the curing and to observe the failure modes as well. Following the experimental raw data on compressive strength, deformability and unit weight have been processed in order to be adopted in the mathematical modelling for interaction and also for general description of the mechanical behaviour.

Preparation of fluid grout has been carried out with bentonite slurry hydratation (duration at least 24 h) and subsequent mixing with retarder, cement and waterglass catalyst, by respecting the mass percentages provided for the standard mix. Both a manual dispersion and a high-speed rotating mixer (up to 8000 rpm) have been adopted during this phase. Weight has been determined by means of 0.01 g precision scale.

Sample preparation has been carried out by using specimen casing where the catalyst has been added to fluid grout and fast rotation of mixer has allowed to disperse and homogenize the grout. Then the casing has been recovered in a box for curing in water. Curing procedure has been selected the following timeline for testing: 1 hour; 24 hours; 7 days; 28 days.

Preparation of specimen requires great care and repeated attempts are necessary to obtain suitable material. This is due to the great sensitivity of final features of the specimen to addition and mixing of water glass. This step has been made with the mentioned high speed mixer in order to be sure that dispersion of water glass is homogeneous and quick inside the grout when still fluid.

213 Grout (without component “B”) viscosity testing with Marsh cone carried out by using a
214 funnel as described in the API Recommended Practice 13B-1 (2014) produced a result
215 between 30 and 45 seconds. Bleeding of the grout (without component “B”) according to
216 the DIN EN 480-4 (2006) was less than 3% at 3 hours. Final mixing of components “A”
217 and “B” produced a total gel time of less than 9 seconds.

218 Uniaxial compression testing has been carried out in a Belladonna mechanical press for
219 soils, equipped with bidirectional displacement rate control device (Fig. 2). Transducers
220 used to measure load and displacements have been respectively a full bridge load cell
221 (CCT model, full scale 5 kN and precision of 1 N) and LVDT devices (HBM models,
222 precision 0.001 mm). Vertical displacement has been measured following the relative
223 movement of the base of the specimen and radial displacements have been measured by
224 using two transducers mounted on opposite and diametral alignment across the specimen.
225 An alternative solution for displacement measurement has not been possible. As the
226 external surface of specimen was not showing adhesive properties and due to the short
227 timeline available between preparation and testing for the majority of specimen, strain
228 gages have not been glued onto the specimen. Radial LVDT transducers have been
229 mounted to be in contact within the medium third of the specimen height.

230 Advancing rate has been adapted in the range of 0.15÷0.45 mm/min and the suitable
231 results have been obtained for the range 0.30÷0.45 mm/min; this selection is a good
232 compromise to avoid creep behavior (excess of lateral swelling) or sudden failure (vertical
233 cracks). Specimen diameter has been selected at 48 mm; for one additional sample the
234 diameter was 52 mm and for two large diameter specimens the value was 75 mm.

Fig. 2 Testing equipment for compression (left) and enlargement of the UCS sample (right). LC: load cell; GS: grout sample; LVDT: radial coupled LVDT transducers; vLVDT: vertical LVDT transducer; PB: base of press plate; RCD: device for advance rate control.

Oedometer testing has been performed by using a standard mechanical oedometer Belladonna equipment (Fig. 3). Ring type has been selected with net diameter of 50 mm and height of 20 mm; this size is sufficient to respect grain size distribution of formed grout. The standard test methods for one-dimensional consolidation properties of soils using incremental loading have been adapted to respect the fact that grout is curing during testing, and thus a compromise was necessary to avoid long term duration typical of oedometer tests in soils (from days to weeks for and an entire loading-unloading cycle).

247 Specimens have been maintained saturated during cycles, and displacement have been
248 measured by means of potentiometric transducers with precision of 0.01 mm.

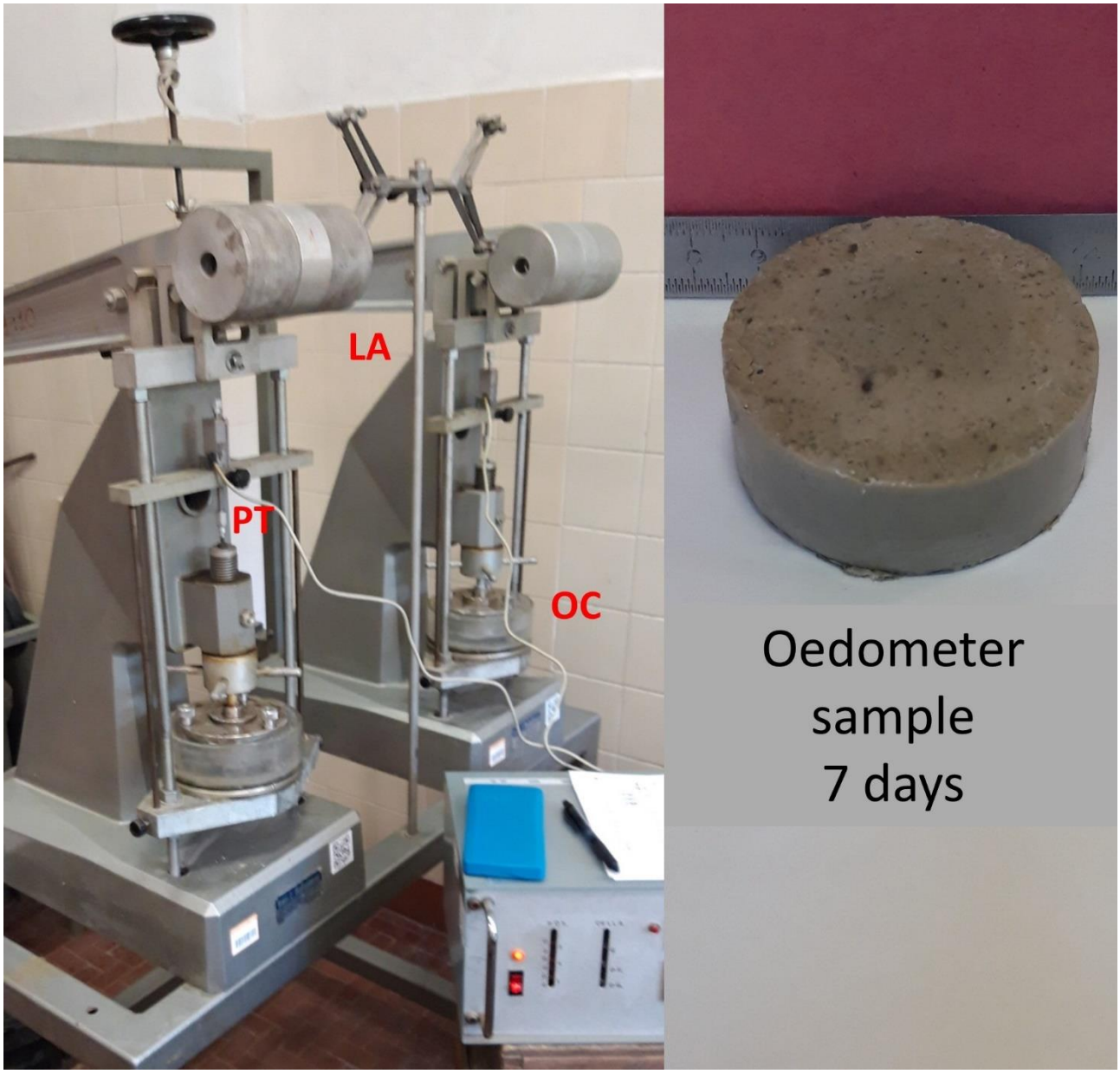

249

250 **Fig. 3. Twin Bishop oedometer equipment used for grout testing (left) and**
251 **oedometer two-component grout sample (right). LA: loading arm; OC: oedometer**
252 **cell with specimen; PT: potentiometric transducer for vertical settlement.**

253 Additional testing has been devoted to obtaining some auxiliary information with the
254 determination of apparent unit weight (geometrical determination, so unit weight has been
255 determined with the geometrical measurement of the volume of specimen casing and of

the weight of ingredients used to fill that volume) and surface strength (by means of soil pocket penetrometer).

Laboratory test results

Compression test results

The main results after uniaxial compression testing are reported in Tab. 1. Strength is considered as the maximum value of stress obtained, for the great majority of cases, at yield at the end of the elastic domain. Deformability values are indexed as secant moduli and Poisson coefficient at 25%, 50% and 75% of the elastic domain and as tangential values at 50% of the elastic domain.

Curing time	Apparent unit weight	UCS	$E_{fm\ s25\%}$	$E_{fm\ s50\%}$	$E_{fm\ s75\%}$	$E_{fm\ t50\%}$	$\nu_{fm\ s25\%}$	$\nu_{fm\ s50\%}$	$\nu_{fm\ s75\%}$	$\nu_{fm\ t50\%}$
1 hour	g/cm^3	MPa	MPa	MPa	MPa	MPa	-	-	-	-
n.1	1.177	0.032	0.95	0.9	0.83	0.75	0.1	0.03	0.06	0.08
n.2	1.198	0.036	2.00	1.6	1.3	1.4	0.19	0.09	0.05	0.03
n.3	1.212	0.024	5.00	2.60	2.40	1.80	0.004	0.07	0.09	0.16
24 hours										
n.1	1.229	0.481	14.4	19.0	21.1	35.2	0.06	0.07	0.06	0.08
n.2	1.179	0.55	18.7	21.5	20.5	25.3	0.05	0.08	-	0.09
n.3	1.201	0.22	10.9	13.2	14.2	17.7	0.09	0.09	0.07	0.07
large diam.75 mm A	1.386	0.53	8.9	11.6	15.0	19.0	-	-	-	-
large diam.75 mm B	1.339	0.41	17.1	20.0	22.7	27.5	-	-	-	-
7 days										
n.1	1.208	0.46	42.3	45.0	40.7	45.0	0.25	0.24	0.22	0.10
n.2	1.214	0.50	23.8	22.9	24.6	32.3	0.02	0.01	-	0.15
n.3	1.099	0.31	23.8	23.5	21.4	24.0	0.06	0.12	-	0.31
n.4	1.271	0.46	17.0	24.5	26.6	42.3	0.17	0.11	-	0.008
7 days, 2nd series										
A	1.270	0.700	34.7	36.7	32.2	32.1	0.02	0.01	0.04	0.004
B	1.270	0.760	21.6	27.4	23.9	56.0	0.32	0.37	-	0.020
large diam.52 mm C	1.248	0.422	33.0	37.0	32.8	38.9	0.11	0.10	0.06	0.06
28 days										

n.1	1.240	0.92	44.4	52.0	55.2	76.7	0.03	0.03	0.04	0.06
n.2	1.233	0.40	10.6	16.9	19.0	34.5	0.15	0.14	0.11	0.12
n.3	1.239	0.84	29.2	37.8	47.7	77.5	0.14	0.10	0.08	0.04
n.4	1.143	0.50	27.6	38.1	39.8	68.6	0.03	0.03	0.05	0.03

Table 1. Results obtained for the two-component grout at different curing timelines in uniaxial condition of compression. Diameter of specimen is usually 48 mm if not indicated. The pedix "s" means secant value, the pedix "t" means tangent value, the pedix "fm" means filling material, UCS: uniaxial compressive strength. Mix components are in the same proportion for the specimen as referred in chapter 2.

In Fig. 4 there is a representative sequence of vertical stress – vertical strain curves at different curing timelines.

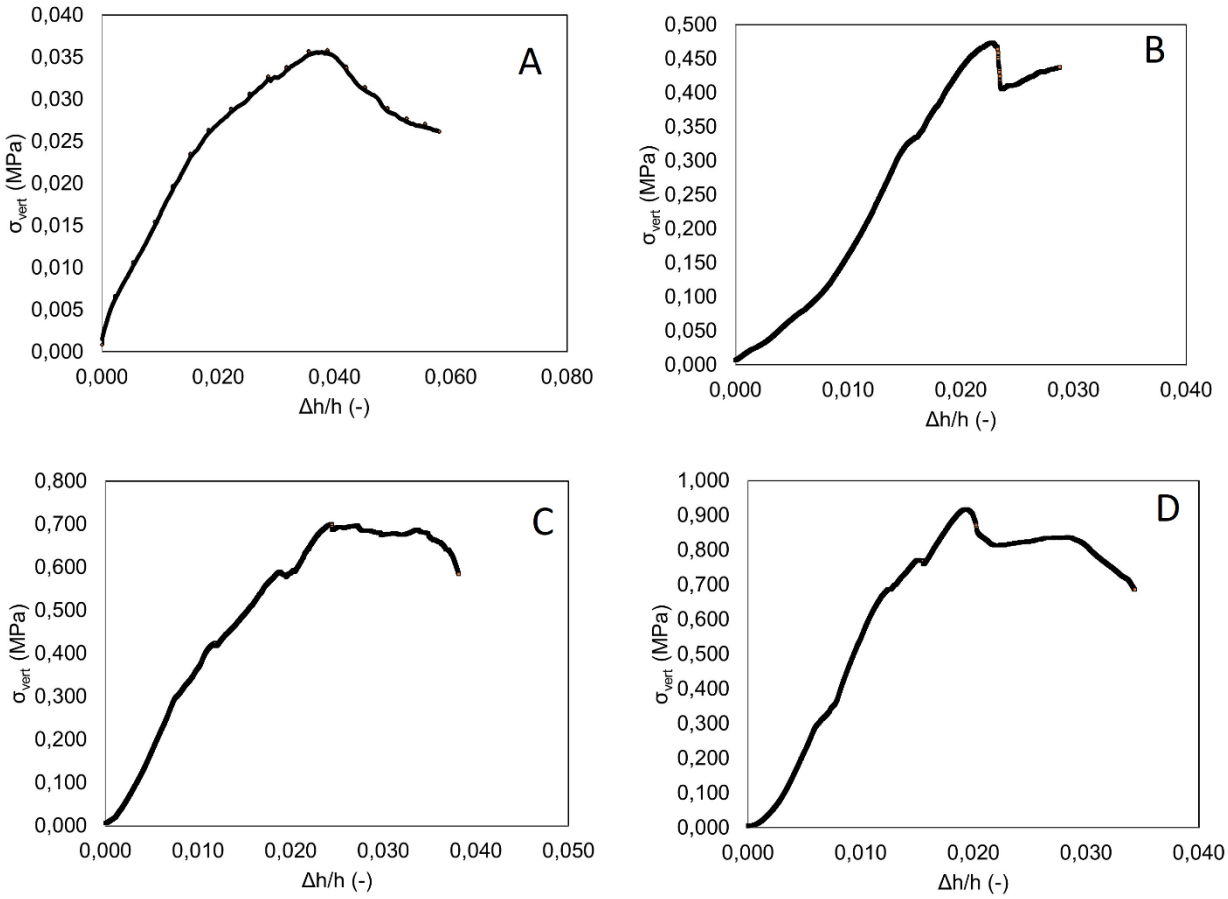

Fig. 4. Vertical stress - strain curves at different curing timelines for the grout. (A) curing time 1 hour, (B) curing time 24 hours, (C) curing time 7 days and (D) curing time 28 days. Each x and y-axis have different scale, adapted for each graph in order to properly show the curve shape. Legend:σ_{vert}: vertical stress; Δh/h: vertical strain, ratio of the vertical displacement on the sample height.

The observed UCS values are rated slightly lower than expected due to the higher amount of retarder introduced. This was intentional, in order to asses also the particular effect of retarder, even if this is not linked to a specific mix design necessarily adopted in practice.

Testing in compression has generally been regular and vertical stress vs. vertical strain is reliable both in the elastic and in the post peak field. A clear yielding and softening behaviour has been observed, with some subvertical and inclined cracks prevailing. In some cases, a pseudoconical shape at failure has been found at the extremities of the specimen, thus respecting the ideal Mohr-Coulomb criterion failure geometry (Fig. 5). The grain size of the cured grout specimens considered as valid appears regular and homogeneous, without veins or lenses at different consistency.

The adoption of a linear Mohr – Coulomb criterion allows one to establish a relationship between the angle of the failure plane α_f and the slope ϕ' of the Mohr Coulomb envelope. The failure angle measured relative to the plane of the major principal stress is:

$$\alpha_f = 45° + \frac{\phi'}{2} \quad (1)$$

In case of UCS of a cohesive material, it is possible also to set:

$$UCS = \frac{2 * c' * cos\phi'}{1 - sin\phi'} \quad (2)$$

The evidence that some of the failed specimens have exhibited a quite defined angle of the failure planes can lead to an estimation of the friction angle and also of the cohesion of the grout.

In Fig. 5 some examples of measured angles at failure are shown; it is necessary to outline that this behaviour has not been clearly observed at the shorter curing time (1 h), probably due to the wide peak and softening of the stress – strain curve in compression that is linked to the distribution of growing cracks of the fresh grout. Easier to be observed at longer curing timelines, where the linear part of the stress–strain curve allows to maintain more defined and extended cracks. Common measured values of α_f are inside the range of 65°÷68, corresponding to values of ϕ' of about 40°÷46°. Due to the relatively small number of tested specimens, it is not still possible to establish a trend of the friction

angle depending on the curing time. It is necessary to outline that shear strength parameters are also depending on the water/cement ratio, on the amount of water glass catalyst and on the percentage of bentonite, clearly variable for each grout mixing type and thus affecting the evolution of such parameters with curing. The raw correspondence among the involved parameters α_f, ϕ', UCS, and c', according to the available data, provides values of c' in the following ranges: after 24hours: 85÷95 kPa; after 7 days: 90÷100 kPa; after 28 days: 135÷155 kPa.

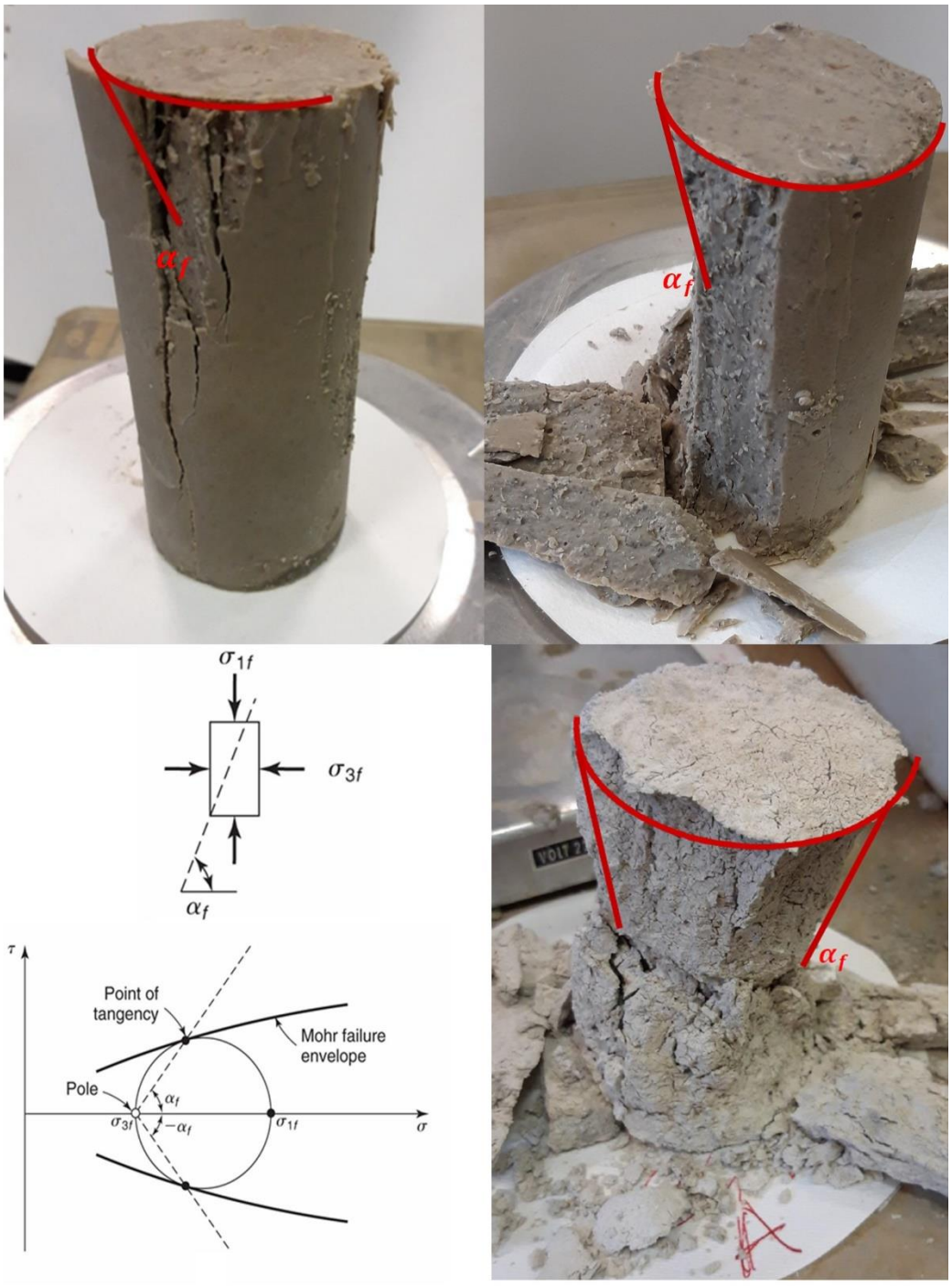

315

316 **Fig.5. Some specimens after failure: on the upper ends the typical conical shape is**
317 **developed and lateral slabbing as well, due to fine and homogenous grain size of**
318 **the grout. The "A" specimen (bottom-right picture) has a diameter of 75 mm and it is**
319 **desiccated. The graphical scheme of the specimen is showing the position of the**
320 **failure plane and the corresponding link with the Mohr failure envelope.**

Figure 6 shows a representative specimen during the compression test and at failure at 28 days curing time. Failure appears as progressive, with slabbing and inclined cracking propagation.

Fig. 6. Sequence of loading and failure after 28 days curing of the grout.

Less easy to be interpreted is the radial strain, at least for two reasons: the first is the possibility to locate the LVDT in the zone of growing microcracks, that can both push out the transducers or to leave them to move inside the crack opening; the second is that, in any case, the greater and compulsory behaviour is clearly following the closure of micropores and damage of cemented structure of the grout, and this happens along the

vertical direction. Concerning the possible evolution of strength parameters, observation are still provisional due to the limited number of tested specimen that cannot allow one to be so confident with characteristic values of strength parameters; preliminary results seems that the greater effect will be on cohesion rather than in friction angle.

Oedometer test results

Confined compression tests can provide essential data in order to understand the behavior of the grout mix, at different curing timelines and at different levels of vertical stress. The fine-grained grout has allowed to use the 50 mm ring diameter as considered to be representative for the geometrical scale of the material. Curing and testing have been carried out in saturated conditions.

During this testing session four curing timelines have been adopted and loading – unloading cycles have been carried out, namely following the following scheme:

- curing 1 hour: 6 new specimens, each of them loaded and unloaded at the respective vertical stress of 50, 100, 200, 400, 800 and 1600 kPa; loading phase has been extended for about 20 minutes, in order to respect the corresponding duration of curing; unloading phase has been driven directly by removing the total applied load for another 20 minutes;
- curing 24 hours: 6 new specimens with the same procedure just described, apart for the duration of loading and unloading phases, which have been extended to 2 hours;
- curing 7 days: 2 new specimens, both loaded at 400 kPa for 6 hours for comparison; then the load on the first specimen has been raised to 1200 kPa for another 4 hours and finally unloaded to zero by measuring displacements for a time

lapse of 2 hours; the second specimen after loading at 400 kPa has been unloaded to zero in a time lapse of 2 hours;

- curing 28 days: 2 new specimens, for comparison, each of them step loaded at the respective vertical stress of 50, 100, 200, 400, 800 and 1600 kPa; loading phase has been extended for about 30 minutes for low loads (that is 50, 100 and 200 kPa, as settlements were stabilized), and for 18 h for higher loads (that is 400, 800 and 1600 kPa); the unloading phase has been stepped by reducing the total applied load to 800 kPa, then 200 kPa and finally to zero, carrying out settlement measurements for 24 hours at each step.

Figure 7 shows some examples of total settlement for the four different adopted curing timelines. The results can be interpreted following the main direction of one dimensional consolidation approach for soils, even a fundamental difference has to be outlined: grout presents a structure which is still chemically reactive and water contained in pores can be pushed aside (classical effect for soil grains) but can also migrate during reaction and therefore the expected properties at rest cannot be fulfilled. The classical approach by Casagrande (1936) can therefore be applied, even if with care.

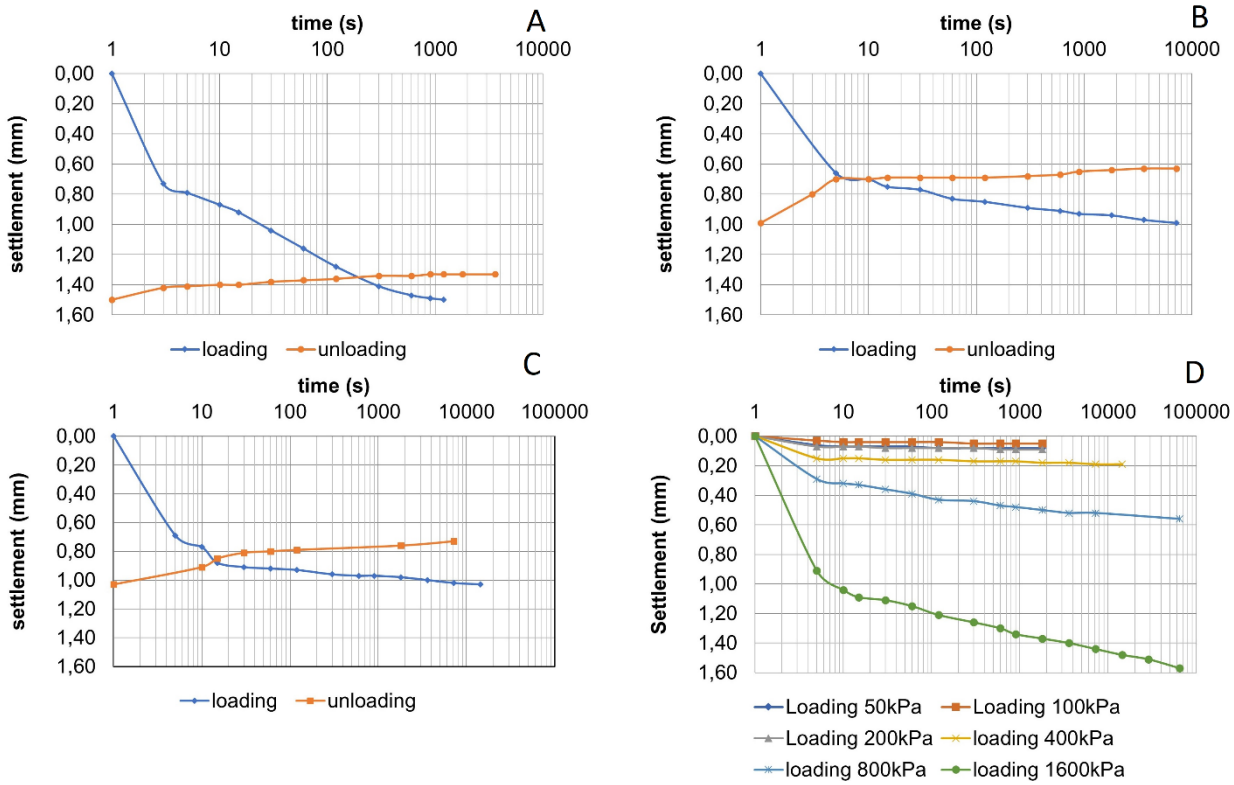

Fig. 7. Example of raw data in log t vs settlement at different grout curing timelines, obtained from oedometer testing (diameter 50 mm and height 20 mm). A) curing time 1 hour under 100kPa load, B) curing time 24 hours under 800kPa load, C) curing time 7 days under 1200kPa load, D) curing time 28 days under all loads.

Figure 8 presents the comparison among the specimens respectively of net strain, due to both mechanical and drainage process of deformation (consolidation), and the total settlement (viscous effects) for two selected curing ages, 1 and 24 hours. These results are interesting because they put in evidence that there is a relevant plastic deformation at the various stress levels, and that is not recoverable, for the various loading levels; the amount of recovered settlement after the unloading phase is low, sometimes negligible. Besides, specimens before and after oedometer test exhibit a clear geometrical change (see Fig. 9).

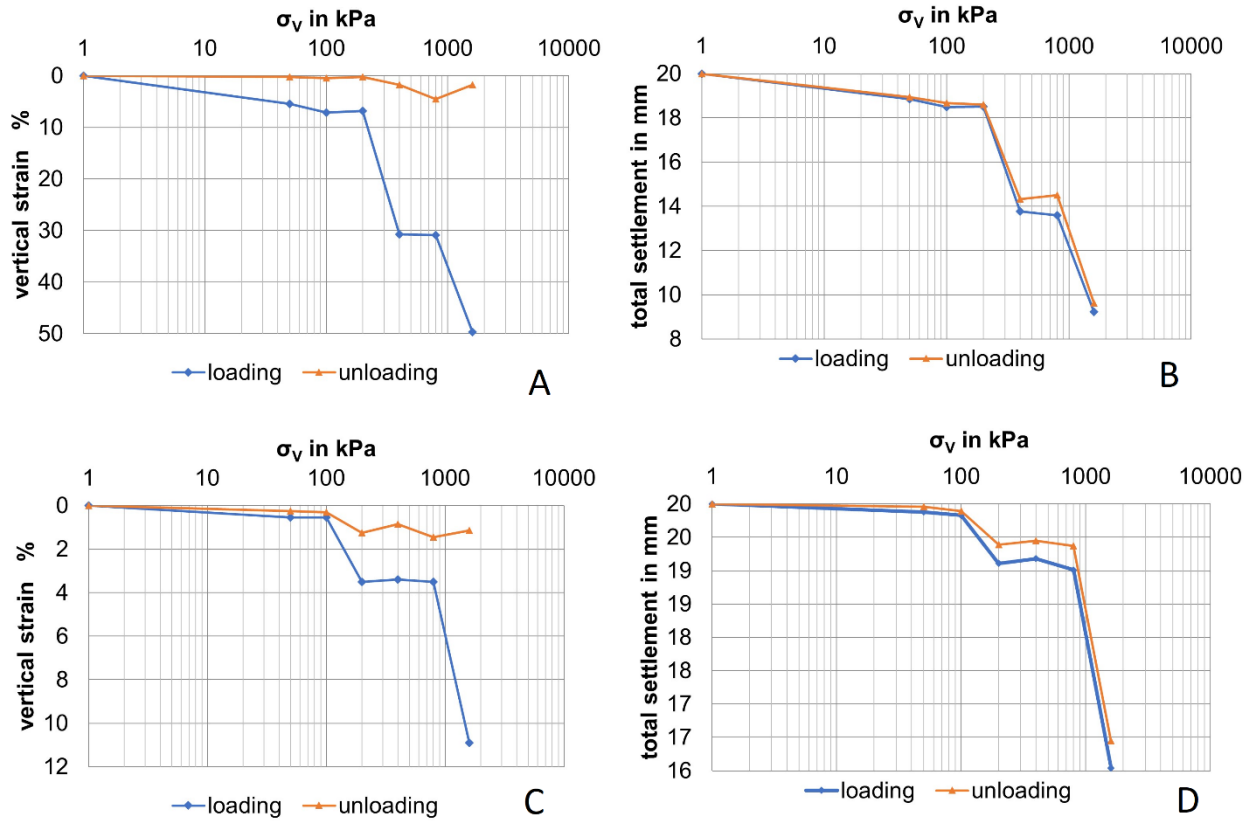

384

385 **Fig. 8. Comparison among the specimens respectively of net strain and total**
386 **settlement at 1 h and 24 h of curing. Net strain values refer to "consolidation" phase**
387 **of loading-unloading, while total settlement refers to the raw values at the beginning**
388 **and at the end of each cycle. A and B refers to 1 hour curing time, C and D to 24**
389 **hours curing time.**

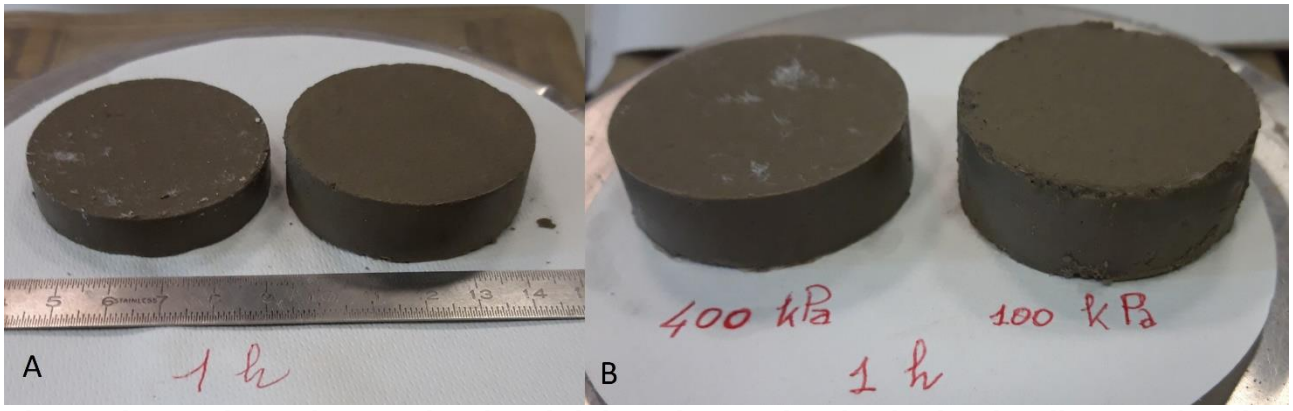

390
391 **Fig.9. A) Specimen before (at the right) and after (at the left) a loading –unloading**
392 **cycle at high stress levels. B) Comparison of specimens after cycle of loading-**

unloading at 100 kPa and 400 kPa: the difference in the residual thickness due to plastic settlements is remarkable.

Figure 10 summarize a typical stress-strain behaviour for the soil-like materials at the end of the curing period (28 days). A critical range of stress for the stability of the grout structure seems to confirm that grout has a meta-stable structure, due to diffusion of bentonite inside the material and to the initial high water/cement ratio.

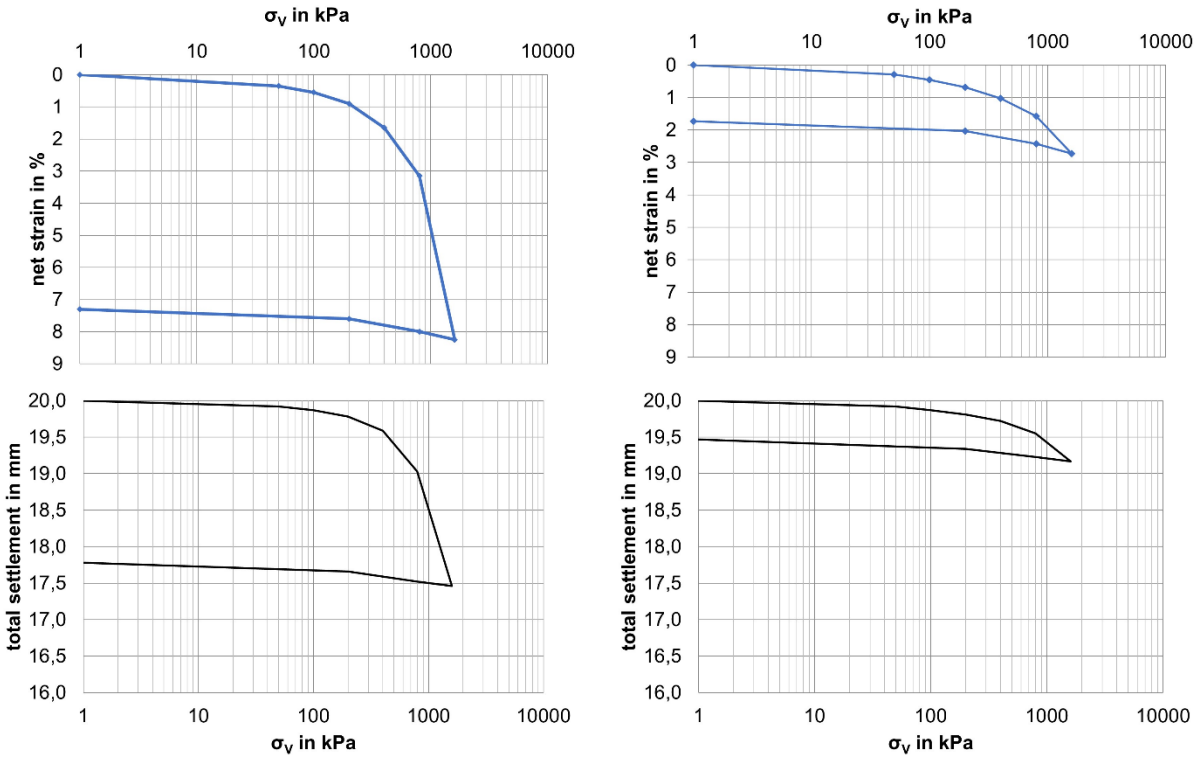

Fig. 10. The diagrams are showing for the two specimens tested after 28 days of curing (OED1, left and OED 2, right) for loading and unloading cycle. Net strain values refer to "consolidation" phase of loading-unloading, while total settlement refers to the raw values at the beginning and at the end of each cycle.

Some interesting features arise from the diagrams showing the values of the constrained moduli, obtained in confined conditions (Fig. 11). It is shown that the curing time is affecting properties of the grout and its workability as well. Strength and stiffness are both

407 “mixing-sensitive”, and this fact should be taken into account for engineering application; in
408 fact, on one side, changes in mixing energy, temperature, moisture and time for mixing
409 can modify the structure, the behaviour and the properties of the grout. On the other side,
410 at the scale of the machine, it is necessary that a suitable compromise is reached for the
411 mixing timing: in fact water glass addition should be operated just to allow the quick setting
412 of the gel and of the cementitious structure, but not so anticipated for the risk of clogging of
413 the grout pipes and nozzles. The final result of a viscous grout to properly fill and support
414 the gap between the lining extrados and the ground excavated profile is the goal.

415 Curing is affecting the values of constrained modulus, as it happened already for the
416 uniaxial compressive test. Moreover, it is interesting that for short curing timelines, a peak
417 value of the modulus appears (namely at 1h and 24 h). This fact seems to be in agreement
418 with the external aspect of the grout, which is similar to a medium consistent clay at the
419 beginning of the curing period, and that reaches the characteristics of a hard soil for long
420 curing time. The presence of these peaks in the modulus graph was well described by
421 Janbu (1969) in the case of fine-grained soils. Its importance is related to the local range
422 of applied stress that is linked to pre-consolidation pressure. It is clear that such
423 phenomenon cannot occur during the preparation of the grout, but this evidence can be
424 interpreted as a “meta-stable pressure” for the grout structure “in formation”. This proposal
425 is quite interesting as it can justify the clear change of behaviour for clay-like conditions of
426 the grout. The similarity to real soil behaviour is arising from the possibility to observe a
427 good adherence to settlement vs time and vertical pressure vs strain of the loading steps
428 of tested grout mix. Moreover the results in Fig.11 concerning the modulus vs the stress
429 level are typical of consolidated clays. That is a convenient reason to make confident to
430 approach with one-dimensional consolidation theory. For sure grout is an artificial material,
431 with cemented bonds that are different from cohesion arising from water suction and

surface membrane effect due to polarity of clay particles: the discussion on such difference should be considered for specific laboratory comparison.

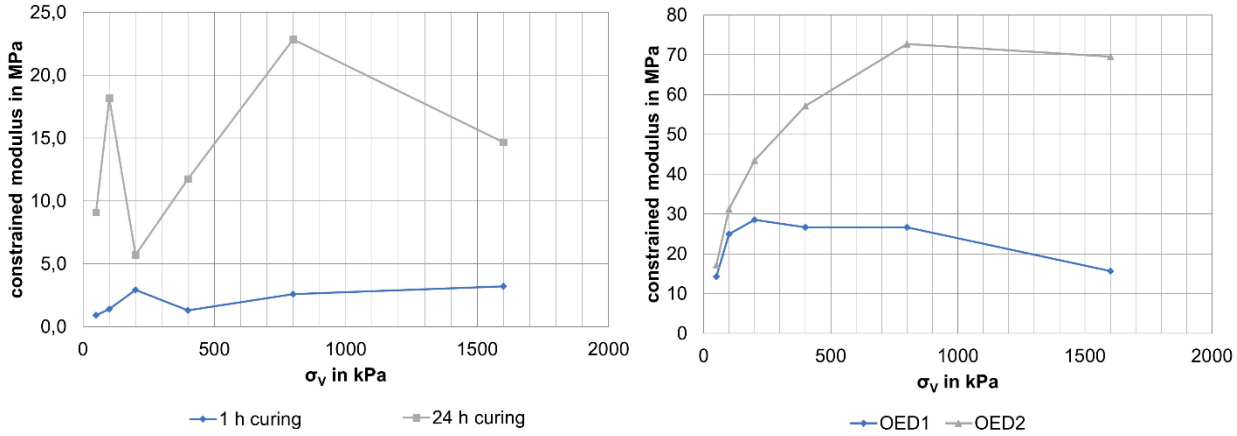

Fig. 11. Scaled graphs showing the distribution of constrained moduli at different curing ages (1 hour and 24 hours at left, 28 days at right) and depending on the vertical applied stress. Note that the y-axis is different to better show the shape of the graphs.

As referred to the original thickness of the specimen (20 mm) and to the specific step in the vertical effective stress ($\Delta\sigma_v$), in the previous graphs the values of the constrained moduli can be considered as tangent values. As far as the constrained modulus is concerned (referring to the full value of applied vertical stress σ_v), after 28 days of curing time the following values have been measured (Tab. 2):

Secant constr. modulus at 28 d in MPa	σ_v 50 kPa	σ_v 100 kPa	σ_v 200 kPa	σ_v 400 kPa	σ_v 800 kPa	σ_v 1600 kPa
OED 1	14.3	18.2	22.2	24.2	25.4	19.4

OED 2	17.2	22.2	29.4	38.4	50.6	58.6

Table 2. The secant values of the constrained moduli at 28 days of curing are listed.

Another relevant issue is concerning the lateral expansion of the grout under loading. Some data arise from the compression testing, showing that the Poisson coefficient "ν" exhibits generally low values. In order to find a confirmation of this behaviour, a correlation between oedometer results and compression results has been arranged, taking into account the basic correlation valid for linear elasticity and for homogenous and isotropic materials in constrained conditions:

$$M_{constr} = \frac{(1-\nu)}{(1+\nu)(1-2\nu)} \cdot E \quad (3)$$

Where M_{constr} is the oedometer modulus, ν is the Poisson ratio and E is the elastic modulus.

The cross checking of the raw data in the uniaxial compression tests and in the oedometer tests allows to obtain values of Poisson coefficient in the range of 0.03÷0.15, confirming the results obtained by direct measures during uniaxial compression tests. The selection of a proper value should follow some criteria such as:

- linearity of the stress – strain envelope;
- type of expected conditions of confinement in the real case;
- level of stress expected in site.

Nevertheless, this appear as one of the most sensitive features of the grout behaviour, thus requesting a larger data base of raw experimental data.

Some additional information can be obtained by means of a further processing of the available data. In order to measure the permeability, it was decided to indirectly obtain through an oedometer test, as for very low permeability values (10^{-8} m/s) it is preferable to use indirect tests (e.g. Colombo and Colleselli, 1996). The indirect coefficient of permeability k can be obtained by as combination of the consolidation coefficient C_V and of the coefficient of volume change m_v by adopting the formula $k = C_V * m_v * \gamma_w$. The intermediate terms can be obtained if some assumptions are taken into account: a) the behaviour of the grout during confined loading is similar to that of fine natural granular materials; b) the interpretation of raw data should follow the one-dimensional consolidation theory; c) the Casagrande method to interpret the rheology of the grout is valid to identify the compressibility features and characteristics of the grout; d) the general limitations on the validity of the indirect coefficient of permeability, known for soils, are maintained also for the artificial grout while carrying out the interpretation of the results. Following these statements, the values of k are presented in the Tab. 3.

Vertical stress in kPa	**1 h curing time**	**24 h curing time**	**7 d curing time**	**28 d curing time OED1**	**28 d curing time OED2**
50	$1.35 \cdot 10^{-7}$	$2.15 \cdot 10^{-7}$	-	$2.75 \cdot 10^{-7}$	$2.85 \cdot 10^{-7}$
100	$4.32 \cdot 10^{-8}$	$7.16 \cdot 10^{-8}$	-	$1.56 \cdot 10^{-7}$	$1.78 \cdot v10^{-7}$
200	$8.87 \cdot 10^{-7}$	$9.41 \cdot 10^{-7}$	-	$2.26 \cdot 10^{-7}$	$1.11 \cdot 10^{-7}$
400	$2.25 \cdot 10^{-8}$	$3.21 \cdot 10^{-7}$	$1.25 \cdot 10^{-7}$ $2.73 \cdot 10^{-9}$	$2.39 \cdot 10^{-7}$	$8.42 \cdot 10^{-8}$
800	$3.35 \cdot 10^{-8}$	$1.63 \cdot 10^{-7}$	-	$2.30 \cdot 10^{-7}$	$6.53 \cdot 10^{-8}$
1200	-	-	$1.29 \cdot 10^{-7}$	-	-
1600	$1.09 \cdot 10^{-8}$	$9.07 \cdot 10^{-8}$		$2.61 \cdot 10^{-7}$	$6.63 \cdot 10^{-8}$

Table 3. Values of indirect theoretical permeability coefficient k in cm/s.

It is important to underline again the fact that the above listed values are obtained through an indirect procedure and not by means of a drainage test. The consequence of this fact is that an interpretation and an engineering judgement is necessary to properly adopt reliable values in practical design. The following issues should be taken into account: a) the order of magnitude of $1.1 \cdot 10^{-7}$ cm/s to $9.4 \cdot 10^{-7}$ cm/s seems reasonable for the majority of tested cases; b) the values at $1.0 \cdot 10^{-8}$ to $9.0 \cdot 10^{-8}$ cm/s are quite optimistic outside the laboratory scale; moreover, settlements and time-dependent movements for both ground and segmental lining can affect the global permeability; c) values in the order of 10^{-9} cm/s seems to be unrealistic. As final consideration, it can be observed that the tested grout has low to very low permeability parameters for a wide range of operational stresses.

Auxiliary testing

Together with data provided in the sheet for cylindrical specimens, some additional information arises from the specimens prepared for oedometer testing. In these cases, apparent unit weight is varying in the range 1.20 to 1.40 g/cm^3 for fresh and cured specimen respectively. Interesting is the reduction of apparent unit weight after loading-unloading cycle for fresh specimen at high level of consolidation pressure: the reduction moves to 0.75 to 1.08 g/cm^3. After drying at natural environmental conditions, apparent unit weight for both cylindrical and disc specimen reduces to less than 0.80 g/cm^3, reaching also 0.71 g/cm^3; desiccated grout is friable and crispy. Soil pocket penetrometer (Soil Test model) has provided, for the first disc specimen, a penetration strength at 1 hour of 90 - 80 - 85 - 80 - 80 - 80 kPa; after 2 hours, the strength was increased to about 120 - 120 - 125 kPa. The second disc specimen presented a penetration strength after 1 hour of about 70 - 60 - 85 kPa, and after 2 hours of about 125 - 150 - 90 - 140 - 90 - 110 kPa. Both specimens after 24 hours reached the full range of the soil pocket penetrometer at more

than 400 kPa; this same result was obtained on the lateral surface of the large diameter cylindrical specimen (75 mm).

3. Simplified methods of tunnel segmental lining analysis

Two methods for the behavior analysis of retaining structures are commonly used in the tunnel field: the convergence-confinement method and the Einstein and Schwartz method (1979). These methods have the advantage of being able to effectively evaluate the complex mechanism of interaction between the support and the walls of the tunnel, using a simplified approach that does not require the use of numerical calculation methods.

More specifically, the convergence-confinement method is able to evaluate the final entity of the loads acting on the support structure, p_{eq} through the intersection of the convergence-confinement curve and the reaction line representing the support structure, determining the displacement of the tunnel wall in the radial direction (u_{eq}) (Fig. 12). The convergence-confinement method is based on the following fundamental assumptions:

- Circular geometry of the tunnel and radial symmetry of the problem analyzed in the two dimensions (vertical section)
- Deep tunnel hypothesis (depth of the tunnel relatively high compared to its radius)
- Homogeneous mechanical characteristics of the rock around the tunnel;
- Hydrostatic initial stress state (undisturbed) p_0 with lateral earth coefficient at rest K_0 = 1.

The main problem in using the convergence-confinement method lies in being able to correctly simulate the three-dimensional nature of the support loading mechanism in a two-dimensional model. The fundamental parameter for this purpose is the displacement u_0 of the tunnel wall when the support structure is installed. Various calculation techniques are

527 available in the literature capable of producing an estimate of this parameter and therefore
528 having reliable results from the convergence-confinement method.

529 Fig. 12 shows the results of the convergence-confinement method through the analysis of
530 two curves: the convergence-confinement curve and the reaction line of the supporting
531 structure. p is the pressure inside the tunnel, acting on the walls, u_R is the radial
532 displacement of the tunnel wall, p_0 is the lithostatic stress present in the rock, u_0 is the
533 radial displacement of the tunnel wall upon installation of the support; p_{eq} and u_{eq} are
534 respectively the final load acting on the support structure and the final displacement of the
535 tunnel wall in the presence of the support structure and u_{max} is the maximum
536 displacement of the tunnel wall in the absence of supports.

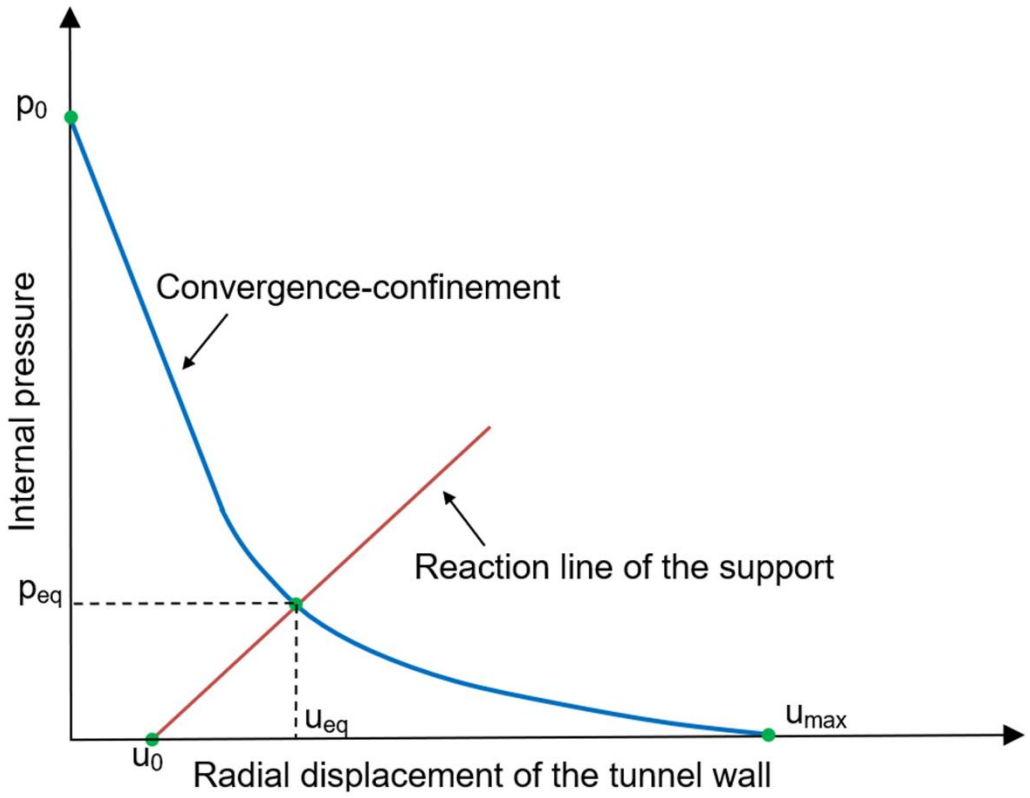

537

Fig. 12 Results of the convergence-confinement method through the analysis of two curves: the convergence-confinement curve and the reaction line of the supporting system.

In the simplest case of ideal elastic-plastic behavior of the rock and Mohr-Coulomb failure criterion, the convergence-confinement curve is expressed by the following relationship (Oreste, 2009):

For $p < \left[p_0 \cdot \left(1 - sin(\varphi)\right) - c \cdot cos(\varphi)\right]$:

$$u_R = \frac{1+\nu}{E} \cdot \left\{ \left[\frac{R_{pl}^{N\Psi+1}}{R^{N\Psi}} \cdot sin(\varphi) + (1 - 2 \cdot \nu) \cdot \left(\frac{R_{pl}^{N\Psi+1}}{R^{N\Psi}} - R \right) \right] \cdot \left(p_0 + \frac{c}{tan(\varphi)} \right) - \frac{1+N_\Phi \cdot N_\Psi - \nu \cdot (N\Psi+1) \cdot (N_\Phi+1)}{(N_\Phi+N_\Psi) \cdot R^{(N_\Phi-1)}} \cdot \left(\frac{R_{pl}^{(N_\Phi+N_\Psi)}}{R^{N\Psi}} - R^{N_\Phi} \right) \cdot \left(p + \frac{c}{tan(\varphi)} \right) \right\} \quad (4)$$

where R_{pl} is the plastic radius of the tunnel:

$$R_{pl} = R \cdot \left[\frac{\left(p_0 + \frac{c}{tan(\varphi)}\right) \cdot \left(1 - sin(\varphi)\right)}{p + \frac{c}{tan(\varphi)}} \right]^{\frac{1}{(N_\Phi - 1)}} \quad (5)$$

$$N_\Phi = \frac{1+sin(\varphi)}{1-sin(\varphi)} \quad (6)$$

$$N_\Psi = \frac{1+sin(\Psi)}{1-sin(\Psi)} \quad (7)$$

R is the tunnel radius, c, φ and Ψ are respectively the cohesion, friction angle and dilatancy of the rock mass, E and ν are respectively the elastic modulus and the Poission ratio of the rock mass.

For $p > \left[p_0 \cdot \left(1 - sin(\varphi)\right) - c \cdot cos(\varphi)\right]$:

$$u_R = \frac{1+\nu}{E} \cdot (p_0 - p) \cdot R \quad (8)$$

The reaction line of the support in the case of a segmental lining must take into account the presence of the filling material in the gap between the segmental lining and the tunnel wall (Fig. 13).

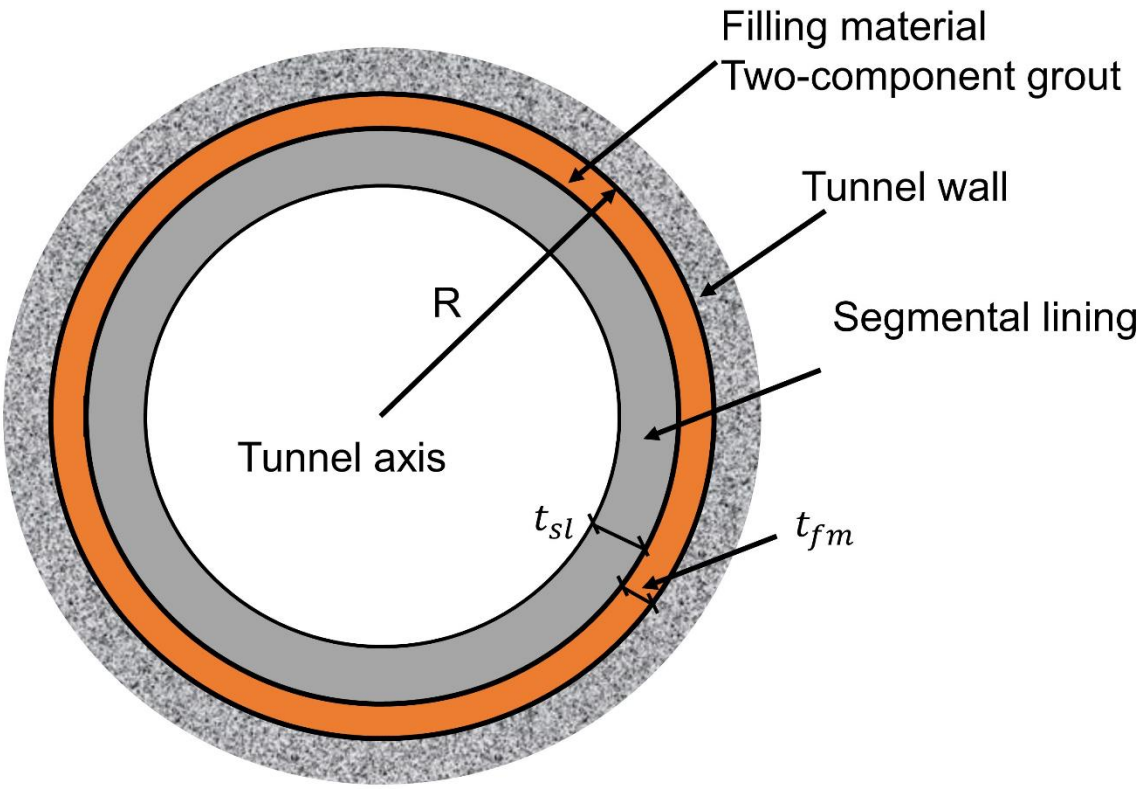

Fig. 13. Geometric sketch of the support system consisting of segmental lining and filling material within a circular tunnel. Legend: R: radius of the tunnel; t_{sl}: thickness of the segmental lining; t_{fm}: thickness of the filling material (not to scale).

Similarly to what was developed for the shotcrete lining plus inner steel set support system (Oreste, 2003; Oreste et al., 2018a, 2018b), it is possible now to define for the reaction line of the support the stiffness, k_{sys}, of the system consisting of the segmental lining and the annulus of the filling material with the following relationship:

$$k_{sys} = \frac{2 \cdot E_{fm} \cdot (1-\nu_{fm}) \cdot R \cdot \left[\frac{E_{fm}}{(1+\nu_{fm})} + (R-t_{fm}) \cdot k_{sl}\right]}{E_{fm} \cdot (1-2 \cdot \nu_{fm}) \cdot R^2 + (R-t_{fm})^2 \cdot \left[E_{fm} + (1-2 \cdot \nu_{fm}) \cdot (1+\nu_{fm}) \cdot k_{sl} \cdot t_{fm} \cdot \left(1 + \frac{R}{(R-t_{fm})}\right)\right]} - \frac{E_{fm}}{(1+\nu_{fm}) \cdot R} \quad (9)$$

where:

$$k_{sl} = \frac{E_{sl}}{(1+\nu_{sl})} \cdot \frac{(R-t_{fm})^2 - (R-t_{fm}-t_{sl})^2}{(1-2 \cdot \nu_{sl}) \cdot (R-t_{fm})^2 + (R-t_{fm}-t_{sl})^2} \cdot \frac{1}{(R-t_{fm})} \quad (10)$$

E_{fm} and ν_{fm} are respectively the elastic modulus and the Poisson's ratio of the filling material; E_{sl} and ν_{sl} are respectively the elastic modulus and the Poisson's ratio of the segmental lining; t_{fm} and t_{sl} are respectively the thickness of the filling material and segmental lining; k_{sl} is the stiffness of the segmental lining. As can be seen from the previous equations, knowing the characteristics of the filling material (thickness, elastic modulus and Poisson's ratio) it is possible to identify the stiffness of the support system which allows to draw the reaction line of the support. In fact, the stiffness of the system represents the inclination of the reaction line with respect to the horizontal axis in the diagram of Fig. 12.

Since the elastic modulus of the filling material E_{fm} varies significantly during the setting period and, therefore, during the loading of the segmental lining, it is necessary to define a representative average value for the considered period. To evaluate it, it is necessary to know not only the trend of the elastic modulus of the filling material over time during the setting period (curing time), but also the advancement speed of the TBM inside the tunnel and the duration of the various excavation and installation of supports. It is a question of addressing this problem with the same approach used for the evaluation of the average elastic modulus of shotcrete during the loading phase of the lining in the tunnel, with the advancement of the excavation phase (e.g. Oreste et al., 2019).

Another very widespread calculation method in the analysis of the behavior of the supporting structures of tunnels is the method of Einstein and Schwartz (1979). This method assumes an annular support continuously connected with the wall of a deep and circular tunnel. Two different cases were examined by the authors: the full slip case and the no-slip case. The solution obtained allows to consider the interaction between the supporting structure and the rock mass around the tunnel, assuming a material with an elastic behavior both for the rock and for the support. For the analysis of the segmental lining with the filling material present in contact with the rock wall, it is more appropriate to refer to the full-slip case, which provides the following equations for the evaluation of the maximum bending moment, M_{max}, and the normal force, N, present in the lining (in particular in the center of the crown and in the middle of the side-wall) (Einstein and Schwartz, 1979; Guan et al., 2015):

$$M_{max} = (1 + \xi) \cdot \frac{p_{eq} \cdot R^2 \cdot (1 - K_0)}{(1 + K_0) \cdot (1 - a_0^*) + (1 - K_0) \cdot (3 - 6 \cdot a_2^*)} \cdot (1 - 2 \cdot a_2^*) \quad (11)$$

$$N_{crown} = \frac{p_{eq} \cdot R \cdot (1 + K_0)}{(1 + K_0) \cdot (1 - a_0^*) + (1 - K_0) \cdot (3 - 6 \cdot a_2^*)} \cdot (2 \cdot a_2^* - a_0^*) \quad (12)$$

$$N_{sidewall} = \frac{p_{eq} \cdot R \cdot (1 + K_0)}{(1 + K_0) \cdot (1 - a_0^*) + (1 - K_0) \cdot (3 - 6 \cdot a_2^*)} \cdot (2 - a_0^* - 2 \cdot a_2^*) \quad (13)$$

where:

$$a_0^* = \frac{C^* \cdot F^* \cdot (1 - \nu)}{C^* + F^* + C^* \cdot F^* \cdot (1 - \nu)} \quad (14)$$

$$a_2^* = \frac{(F^* + 6) \cdot (1 - \nu)}{2 \cdot F^* \cdot (1 - \nu) + 6 \cdot (5 - 6 \cdot \nu)} \quad (15)$$

$$C^* = \frac{E \cdot R \cdot (1 - \nu_s^2)}{E_s \cdot A_s \cdot (1 - \nu^2)} \quad (16)$$

$$F^* = \eta \cdot \frac{E \cdot R^3 \cdot (1-\nu_s^2)}{E_S \cdot I_S \cdot (1-\nu^2)} \quad (17)$$

p_{eq} is vertical load acting on the support structure in the vertical direction, in correspondence with the crown tunnel (evaluated, for example, through the convergence-confinement method);

K_0 is the lateral earth pressure at rest in the rock, in the initial undisturbed conditions;

R is the tunnel radius;

E and ν are respectively the elastic modulus and the Poisson ratio of the rock;

E_s and ν_s are respectively the elastic modulus and the Poisson ratio of the support structure;

A_s and I_s are respectively the area and moment of inertia of the cross section of the support, through a plane passing through the axis of the tunnel. The cross section therefore has a rectangular section, whose width is equal to 1 m in the direction of the tunnel axis and the height is equal to the thickness of the support

C^* and F^* are compressibility ratio and flexibility ratio of the support, respectively.

ξ is the incremental coefficient that takes into account the transfer of stresses from one ring to the adjacent one, in correspondence with the longitudinal joints of the segmental lining. Guan et al. (2015) were able to note how this parameter varies from 0.44 to 0.46, with an intermediate value equal to 0.45 and is not influenced by the characteristics of the ground and the depth of the tunnel, but only by the geometric and mechanical characteristics of the longitudinal and transverse joints of the segmental lining;

η is reduction coefficient taking into account the presence of longitudinal joints in segmental lining. In this regard Guan et al. (2015) suggest reducing the bending stiffness by a coefficient η, which was found to vary between 0.4 and 0.7, with an intermediate value of 0.55. This coefficient was found to be higher in more compact soils and for tunnels at greater depths.

The maximum moment M_{max} assumes the same value in the center of the crown and on the sidewall, but a different sign: the one in the crown will be considered positive and the one on the sidewall negative, for the typical case in which K_0 is less than 1; if K_0 is greater than 1, the moment on the sidewall will be positive and the moment at the crown tunnel is negative.

The normal forces are different in the tunnel crown and on the sidewall: by associating the values of the normal forces with the bending moments, it is possible to check the hypothesized lining in the two critical points highlighted above: the center of the crown tunnel and the center of the. In the verification process, the thickness of the segmental lining is changed to obtain a value considered compatible with the safety and stability conditions of the support structure and the tunnel.

When the use of segmental lining as a support structure is planned, it is important to consider composite support is obtained which also includes a ring of filling material between the segmental lining and the wall of the tunnel. The evaluation of the equivalent elastic modulus of the support must consider the presence of the two materials (Fig. 13). Assuming the preservation of the flat sections of the lining (segmental lining and filling material), it is possible to identify the equivalent elastic modulus $E_{s,eq}$ of the support. This equivalent elastic modulus turns out to be different in relation to the bending and

compression of the lining and, therefore, must be evaluated through different equations with reference to the compressible ratio C^* and the flexibility ratio F^*.

Equivalent elastic modulus of the support with reference to the compressibility ratio C^*:

$$E_{s,eq(C^*)} = E_{sl} + E_{fm} \cdot \frac{t_{fm}}{t_{sl}} \tag{18}$$

Equivalent elastic modulus of the support with reference to the flexibility ratio F^*:

$$E_{s,eq(F^*)} = \frac{4}{t_{sl}^3} \cdot \left\{ E_{sl} \cdot [y_0^3 + (t_{sl} - y_0)^3] + E_{fm} \cdot \left[\left(t_{sl} + t_{fm} - y_0\right)^3 - (t_{sl} - y_0)^3 \right] \right\} \tag{19}$$

Where:

$$y_0 = \frac{E_{sl} \cdot t_{sl}^2 + E_{fm} \cdot \left(t_{fm}^2 + 2 \cdot t_{sl} \cdot t_{fm}\right)}{2 \cdot \left(E_{sl} \cdot t_{sl} + E_{fm} \cdot t_{fm}\right)} \tag{20}$$

Being y_0 the distance of the neutral axis of the section from the intrados of the segmental lining.

The values of the equivalent elastic modules reported above were obtained assuming an equivalent support of thickness equal to the thickness of the segmental lining: $t_{s,eq} = t_{sl}$. For this reason, the values of the area of the support section A_S and of the moment of inertia I_s must be evaluated with the following two equations:

$$A_s = b_s \cdot t_{sl} \tag{21}$$

$$I_s = \frac{b_s \cdot t_{sl}^3}{12} \tag{22}$$

Where b_s is the width of the support section in the direction of the tunnel axis, considered equal to 1 m.

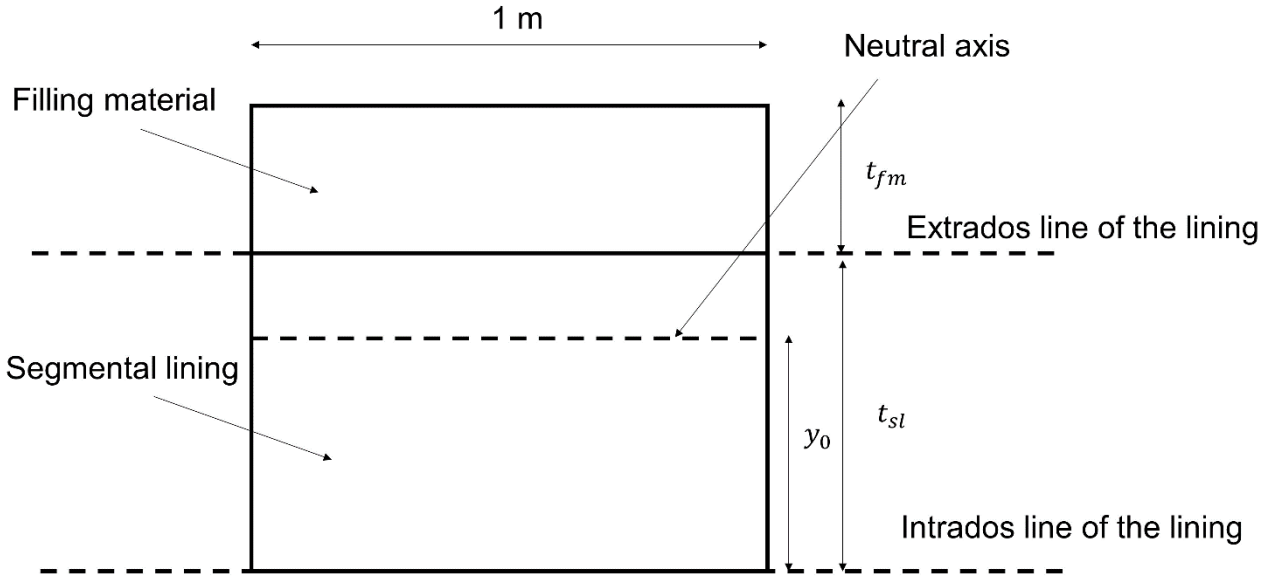

668

669 **Fig. 14. Cross section of the segmental lining with the presence of the filling**
670 **material. Legend: t_{sl} is thickness of the segmental lining; t_{fm} is thickness of the**
671 **filling material; y_0 is distance of the neutral axis of the section from the intrados of**
672 **the segmental lining.**

673 Based on the calculations that can be developed considering the equivalent support
674 described above, it will be possible to identify the maximum moments along the
675 development of the support and the normal forces at the center of the crown and the
676 sidewall. Starting from these results, it will be possible to determine the circumferential
677 stresses σ_ϑ in the segmental lining and in the filling material using the following equations.

678 Circumferential stress at the extrados of the segmental lining $\sigma_{\vartheta,sl,ex}$ due to moment M:

679 $$\sigma_{\vartheta,sl,ex} = \frac{12 \cdot M}{E_{s,eq(F^*)} \cdot b_s \cdot t_{sl}^3} \cdot (t_{sl} - y_0) \cdot E_{sl} \quad (23)$$

680 Circumferential stress at the intrados of the segmental lining $\sigma_{\vartheta,sl,in}$ due to moment M:

681 $$\sigma_{\vartheta,sl,in} = -\frac{12 \cdot M}{E_{s,eq(F^*)} \cdot b_s \cdot t_{sl}^3} \cdot y_0 \cdot E_{sl} \quad (24)$$

Maximum circumferential stress on the extrados of the filling material $\sigma_{\vartheta,fm,ex}$ due to the moment M:

$$\sigma_{\vartheta,fm,ex} = \frac{12 \cdot M}{E_{s,eq(F^*)} \cdot b_s \cdot t_{sl}^3} \cdot \left(t_{fm} + t_{sl} - y_0\right) \cdot E_{fm} \tag{25}$$

Constant stress in the segmental lining section due to the normal force N:

$$\sigma_{\vartheta,sl} = \frac{E_{sl}}{E_{s,eq(C^*)}} \cdot N \tag{26}$$

Constant stress in the section of the filling material due to the normal force N:

$$\sigma_{\vartheta,fm} = \frac{E_{fm}}{E_{s,eq(C^*)}} \cdot \frac{t_{fm}}{t_{sl}} \cdot N \tag{27}$$

The stress effects of the bending moment M and the normal force N must be summed algebraically to obtain the overall stress state in the filling material and in the segmental lining; in addition to the circumferential stresses, the radial stresses present in the two materials must be considered: p_{eq} at the extrados of the filling material and segmental lining and 0 at the intrados of the segmental lining. The overall stress state has to be compared to the strength of the material (the limit stress state), according to the Mohr-Coulomb strength criterium:

$$\sigma_{lim} = UCS + \frac{1+sin(\varphi)}{1-sin(\varphi)} \cdot \sigma_r \tag{28}$$

Where UCS and φ are respectively the uniaxial compression strength and the friction angle of the material (concrete or filling material) and σ_r is the radial stress in the point where the stress state is evaluated during the design of the support structure (extrados of the filling material annulus, extrados or intrados of the segmental lining).

The knowledge of the overall stress state in the critical points of the support system allows to proceed to the verifications regarding the strength of the materials and, therefore, to the design of the segmental lining through the definition of its thickness and the internal reinforcement necessary to absorb the developing bending moments.

4. The effect of the two-component grout on the behavior of the tunnel segmental lining

From the laboratory tests on the two-component grout used as filling material, it is possible to detect how the value of the Poisson's ratio remains relatively low and uncertain (variable in the range 0.03-0.15) during the curing time. Besides, both the elastic modulus of the material and the UCS show a complex trend over time, described by the trends shown in Figs. 15 and 16. The values plotted in the figures are the average values between those measured in the laboratory tests of uniaxial compression for the different maturation times analyzed: 1 h (i.e. 0.04167 d), 1 day, 7 days, 28 days.

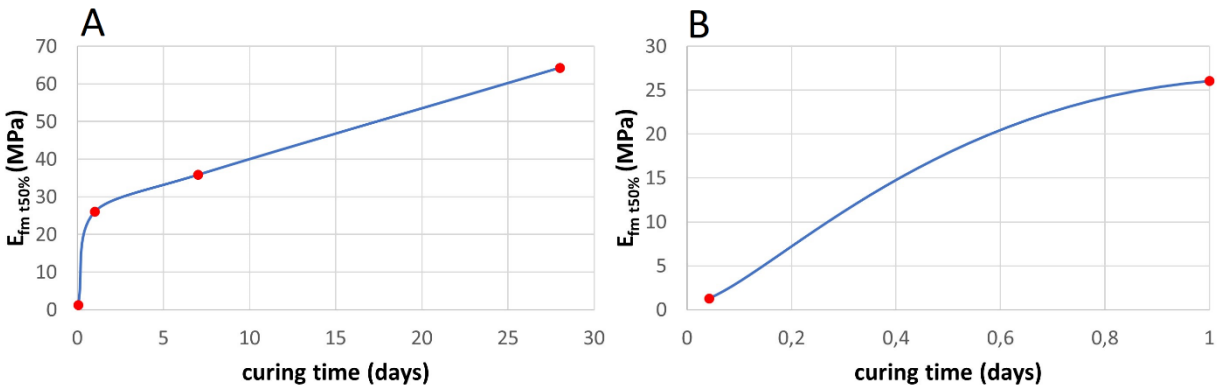

Fig. 15. Trend of the tangent elastic modulus for a stress state equal to 50% of the uniaxial compressive strength ($E_{fm,t\ 50\%}$) as the curing time varies. A): full time interval (0-28 days); B): detail on the first day of curing time (0-1 days).

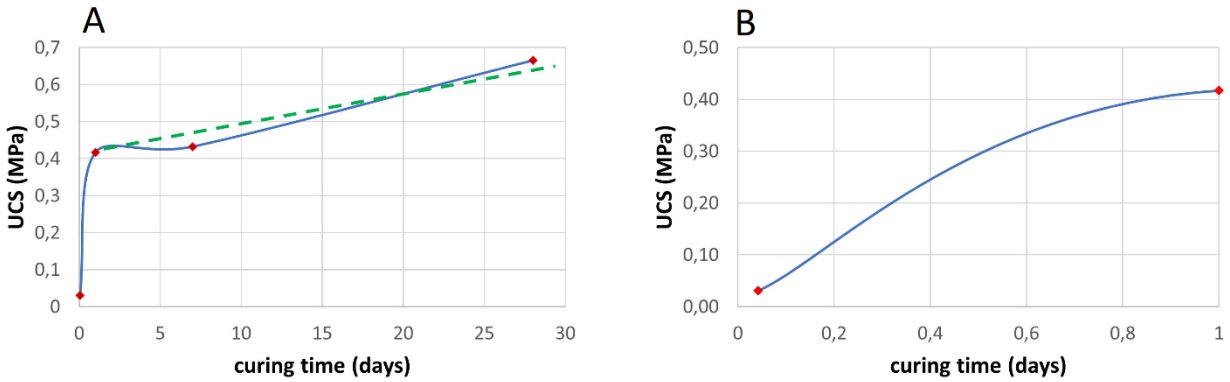

718

719 **Fig. 16. Trend of uniaxial compressive strength (UCS) as the curing time varies. A):**
720 **full time interval (0-28 days); B): detail on the first day of curing time (0-1 days).**
721 **Legend: dotted line: hypothetical linear trend for the period following the first day of**
722 **curing.**

723 More specifically, it is possible to hypothesize for the elastic modulus and for the UCS a
724 strong increase in the first day of curing and a linear trend for the subsequent period, up to
725 the 28 days of curing. On the first day of curing, it is plausible to hypothesize a parabolic
726 trend of the curves shown in the previous figures (Figs. 15 and 16). Assuming that the
727 parabolic curves connect with the straight lines for a curing time equal to 1 day and that
728 the additional condition that set UCS and $E_{fm,t\ 50\%}$ zero for the time equal to t = 0 is valid,
729 we obtain the following equations that allow us to describe the trends of the elastic
730 modulus and of the UCS over time, according to the parabola-trapezium scheme.

731 $E_{fm,t\ 50\%}$ in the period 0-1 day:

732 $$E_{fm\ t50\%} = -5{,}7713 \cdot t^2 + 31{,}839 \cdot t \quad (29)$$

733 $E_{fm,t\ 50\%}$ in the period 1-28 days:

734 $$E_{fm\ t50\%} = 1{,}4274 \cdot (t-1) + 26{,}0667 \quad (30)$$

735 UCS in the period 0-1 day:

736 $$UCS = -0{,}3329 \cdot t^2 + 0{,}74989 \cdot t \quad (31)$$

737 UCS in the period 1-28 days:

738 $$UCS = 0{,}0089 \cdot (t - 1) + 0{,}417 \quad (32)$$

739 The identification of the average elastic modulus of the E_{fm} of the filling material during the
740 loading of the segmental lining (with the advancement of the excavation face) is of great
741 importance, as this parameter has a great influence on the stiffness of the k_{sys} system
742 and, therefore, on the load induced on the segmental lining (Fig. 12). Another fundamental
743 parameter is the thickness of the filling material t_{fm}. In order to investigate the influence of
744 these parameters and the Poisson's ratio of the filling material ν_{fm} a parametric analysis
745 was developed, proceeding with the calculation of the stiffness of the k_{sys} system (eq. 9)
746 considering all the following values of the influencing parameters, within the ranges of
747 variability obtained from the laboratory tests described in this paper or from the scientific
748 literature:

749 - Tunnel radius R: 2, 3.5 and 5 m;
750 - Elastic modulus of the filling material E_{fm}: 15, 30 and 45 MPa;
751 - Poisson's ratio of the filling material ν_{fm}: 0.03, 0.09 and 0.15;
752 - Thickness of the filling material t_{fm}: 0.12, 0.18 and 0.24 m;
753 - Thickness of the segmental lining t_{sl}: 0.3 and 0.4 m.

754 For the concrete forming the segmental lining, an elastic modulus E_{sl} of 30,000 MPa and a
755 Poisson's ratio ν_{sl} of 0.15 were considered. On the basis of the 162 analyzes carried out, it
756 was possible to detect how the Poisson's ratio of the filling material has little influence on

757 the stiffness k_{sys} of the system in all the examined cases. For this reason, it is possible to
758 plot the results obtained by neglecting this parameter, assuming it equal to 0.09, the
759 intermediate value of the variability interval detected by laboratory tests (0.03-0.15).

760 Figure 17 (A and B) shows the values of the stiffness of the support system k_{sys} as the
761 radius of the tunnel R varies, for the different values of E_{fm} and t_{fm} considered,
762 respectively for a thickness of the segmental lining of 0.3 and 0.4 m.

763

764

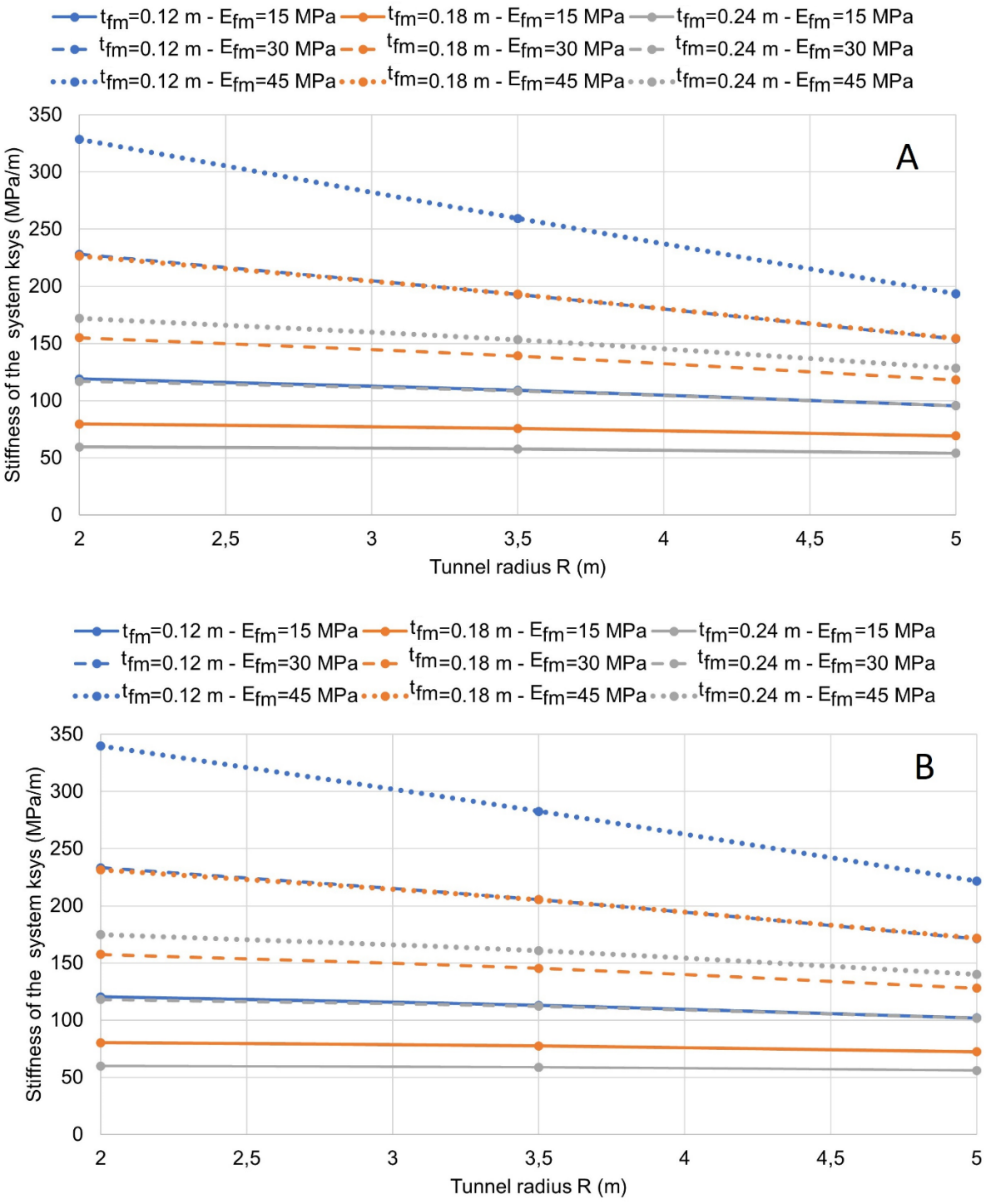

765

766 **Fig. 17. Trend of the stiffness of the support system (segmental lining + filling**
767 **material annulus) k_{sys} as the tunnel radius R varies, for different values of the elastic**
768 **modulus E_{fm} and the thickness t_{fm} of the filling material, for the case of segmental**
769 **lining with a thickness of 0.3 m (A) and 0.4 m (B).**

From Fig. 17, it can also be seen that the radius of the tunnel R does not have a detectable influence on the stiffness of the system when the values of E_{fm} are low and those of t_{fm} high. Furthermore, for small tunnel radii, the thickness of the segmental lining does not affect the rigidity of the system. Once the correct value of the stiffness of the k_{sys} system has been identified from the graphs of Fig. 17, it is possible through the convergence-confinement method to obtain an estimate of the load p_{eq} acting on the support system, in order to proceed with the design of the segmental lining and the definition of its thickness. In some cases, it is necessary to limit the load acting on the support system, to avoid an excessive stress state induced in the concrete constituting the segmental lining. This is the case of tunnels at great depths, for which it is possible to intervene appropriately on the thickness of the filling ring (increasing it) and on the mechanical characteristics of the filling material (limiting the elastic modulus) in order to obtain a low k_{sys} stiffness and, therefore, reduced load values on the support system.

In order to obtain a low elastic modulus value of the filling material, appropriate additives (e.g. higher retarder dosage) of the two-component material can be used or the excavation machine's advancement speed can be increased (if the technical conditions allow it), in order to load the segmental lining in relatively short times, when still the filling material shows limited mechanical parameters.

The design of the segmental lining proceeds with calculation methods that allow to study the development of the bending moments and of the axial forces along the development of the support, starting from the load p_{eq} that can be evaluated with the convergence-confinement method. Among the most common is the method of Einstein and Schwartz (1979), whose stiffness parameters C^* and F^* (the compressibility ratio and flexibility ratio of the support, respectively) were illustrated previously.

Also in this case, an extensive parametric analysis has been developed on the parameters that influence the coefficients C^* and F^* in order to verify the effect of the presence of the filling material on the behavior of the support structure.

The same values already used in the analysis relating to the stiffness k_{sys} of the system have now been adopted, with the addition of 3 different values of the elastic modulus of the rock mass: 3,162 MPa (relative to a rock mass having GSI = 30), 10,000 MPa (GSI = 50) and 31,622 MPa (GSI = 70), where GSI is the Geological Strength Index of the rock mass (Hoek, 1994; Hoek et al., 1995; Hoek and Brown, 1997; Serafim and Pereira, 1983) .

The total of the performed analyzes was therefore equal to 486. It was possible to verify that in all cases the effect of the presence of the filling material ring is always less than 1.5 ‰ on parameter C^* and always less than 1.5% on parameter F^*. In practical terms, therefore, in the analysis of the behavior of segmental lining through the Einstein and Schwartz method, it is possible to neglect the presence of the filling material ring in the evaluation of bending moments and normal forces acting on segmental lining. The design of the segmental lining can therefore proceed quickly, evaluating the stress state induced in the segmental lining, for different values of its thickness, after having calculated the acting bending moments and the normal forces.

5. Conclusions

Where a two-component grout is used during TBM excavation, the mechanical properties evolve over the time immediately after the injection, just during the loading of the linings. It is, therefore, important to be able to analyze the mechanical behavior of this filling material, in order to evaluate the effects of its presence on the stress state induced in segmental lining. An extensive laboratory program has been performed considering a particular mix-design of a two-component grout. Uniaxial compression tests and

oedometer tests, were carried out and allowed to characterize this type of material from a mechanical point of view over time. In particular, the stiffness (elastic modulus, Poisson's ratio, oedometer modulus) and the strength parameters (uniaxial compressive strength, friction angle and cohesion) were evaluated during the curing period of the material. The test campaign showed a certain sensitivity of the material to the preparation methods of the mixture and in particular in the gel formation phase with the mixing of the two components. The material presents a relatively modest density of the material obtained, due to a relatively high water/cement ratio, an elastic-plastic behavior of the material of the "softening" type, and specific compression threshold levels observed in the oedometer test, beyond which water seems to be expelled from the pores and a failure of the solid skeleton previously formed appears, with the consequent appearance of irreversible deformations.

Constrained compression has shown the role of a metastable structure in the formed grout, that determines a change of the settlement rate when a transition pressure is reached (meta stable pressure).

A detailed analysis of the influence of the filling material on the behavior of segmental lining was carried out using two widespread methods of calculating the tunnel support structures: the convergence-confinement method and the Einstein and Schwartz (1979) method. In particular, for the convergence-confinement method, the stiffness of the support system (segmental lining + filling ring) was evaluated. It has been noted how this stiffness of the support system can significantly affect the value of the load acting on the segmental lining. For the method of Einstein and Schwartz the stiffness coefficients of the lining were obtained, taking into account the presence of the filling material ring. An extensive parametric analysis allowed to identify the effects of the presence of the filling material in the two calculation methods considered. From the study carried out it was

possible to detect how the filling material has a significant effect on the stiffness of the support system in the convergence-confinement method and, therefore, on the load acting on the segmental lining. Instead, it has reduced and even negligible effects on the overall stiffness of the support system in the Einstein and Schwartz method used to carry out a first design of the segmental lining. With this latter calculation method, the analysis can proceed neglecting the presence of the filling material ring and directly obtaining the stresses affecting the segmental lining by adopting the stiffness parameters relating solely to segmental lining.

Acknowledgment

The authors wish to thank Master Builders Solutions for the permission granted to publish the results.

Conflict of interests

Authors declare they have no conflict of interest.

References

API Recommended Practice 13B-2 (2014). Recommended Practice for Field Testing Oil-Based Drilling Fluids. American Petroleum Institute.

Beghoul, M. and Demagh, R. (2019). Slurry shield tunneling in soft ground. Comparison between field data and 3D numerical simulation. Studia Geotechnica et Mechanica, 41(3), 115–128.

Bezuijen, A. and Talmon, A. (2003) Processes around a TBM. Geotechnical Aspects of Underground Construction in Soft Ground, 48–56, 2008. doi: 10.1201/9780203879986.ch1.

866 Casagrande, A. (1936). The determination of the pre-consolidation load and its practical
867 significance. Proceedings of the international conference on soil mechanics and
868 foundation engineering. 3. Harvard University Cambridge, 60–64.
869 Colombo, P., and Colleselli, F. (1996). Elementi di Geotecnica, Zanichelli, Bologna (in
870 Italian).
871 Dai, Z., Bai, Y., Peng, F., and Liao, S. (2010). Study on mechanism of simultaneous
872 backfilling grouting for shield tunnelling in soft soils. GeoShanghai Int. Conf. on Deep and
873 Underground Excavations, ASCE, Reston, VA, 182–190.
874 Deutscher Ausschuss für unterirdisches Bauen e. V. (DAUB) (2013). Recommendations
875 for the design, production and installation of segmental rings. Deutscher Ausschuss für
876 unterirdisches Bauen e. V. (DAUB).
877 Dias, T.G.S. and Bezuijen, A. (2015). TBM Pressure Models - Observations, Theory and
878 Practice. 15th Pan-American Conference on Soil Mechanics and Geotechnical
879 Engineering - Geotechnical Synergy in Buenos Aires 2015, 347–374, 2015. doi:
880 10.3233/978-1-61499-599-9-347.
881 DIN EN 480-4 (2006). Admixtures for concrete, mortar and grout - Test methods - Part 4:
882 Determination of bleeding of concrete. Deutsche Institut für Normung e.V., Beuth Verlag,
883 Berlin.
884 Do, N.-A., Dias, D., Oreste, P., Djeran-Maigre, I. (2014a). 2D Tunnel Numerical
885 Investigation: The Influence of the Simplified Excavation Method on Tunnel Behaviour.
886 Geotechnical and Geological Engineering, 32, 1, 43-58.
887 Do, N.A., Dias, D., Oreste, P., Djeran-Maigre, I. (2014b). 2D numerical investigations of
888 twin tunnel interaction. Geomechanics and Engineering, 6(3), pp. 263-275.
889 Do, N.-A., Dias, D., Oreste, P., Djeran-Maigre, I. (2015). 2D numerical investigation of
890 segmental tunnel lining under seismic loading. Soil Dynamics and Earthquake
891 Engineering, 72, 66-76

892 Do, N.-A., Dias, D., Oreste, P. (2016). 3D numerical investigation of mechanized twin
893 tunnels in soft ground - Influence of lagging distance between two tunnel faces.
894 Engineering Structures 109, 117-125.
895 Einstein, H.H. and Schwartz, C.W. (1979). Simplified analysis for tunnel supports. J.
896 Geotechnical Eng. Division ASCE, 105(4), 499-518.
897 Flores, A.Q. (2015). Physical and mechanical behavior of a two component cement-based
898 grout for mechanized tunneling application. MSc Thesis, Universidade Federal do Rio de
899 Janeiro, Brazil.
900 Guan Z., Deng T., Wang G. and Jiang Y. (2015). Studies on the key parameters in
901 segmental lining design. Journal of Rock Mechanics and Geotechnical Engineering, 7,
902 674-683.
903 Hashimoto, T., Brinkman, J., Konda, T., Kano, Y., and Feddema, A. (2004). Simultaneous
904 backfill grouting, pressure development in construction phase and in the long-term.
905 Underground space for sustainable urban development. Proceedings of the 30th ITA-
906 AITES World Tunnel Congress, 19, 4–5, 447.
907 Hirata, T. (1989). Study on behavior of cohesive soil in type shield tunneling work and on
908 construction technique. Doctoral Thesis, Kyoto University, Japan.
909 Janbu N. (1969) The resistance concept applied to deformations of soils. In: The 7th
910 International Conference in Soil Mechanics and Foundation Engineering, Mexico, 191–
911 196.
912 Hoek, E. (1994). Strength of rock and rock masses. ISRM News Journal, 2(2), 4-16.
913 Hoek, E., Kaiser, P.K. and Bawden, W.F. (1995). Support of underground excavations in
914 hard rock. Rotterdam, Balkema.
915 Hoek, E. and Brown, E.T. (1997). Practical estimates or rock mass strength. Int. J. Rock
916 Mech. & Mining Sci. & Geomechanics Abstracts, 34(8), 1165-1186.

917 Komiya, K., Soga, K., Akagi, H., Jafari, M.R. and Bolton, M.D. (2001). Soil consolidation
918 associated with grouting during shield tunnelling in soft clayey ground. Geotechnique, 51,
919 10, 835-846.
920 Lee, K. M., Rowe, R. K. and Lo, K.Y. (1992). Subsidence owing to tunneling. I. Estimating
921 the gap parameter. Canadian Geotechnical Journal, 29, 929–940.
922 Maidl, B., Herrenknecht, M. and Anheuser, L. (1995). Mechanised Shield Tunnelling. Ernst
923 & Sohn, Berlin.
924 Ochmański, M., Modoni, G. and Bzówka, J. (2018). Automated numerical modelling for the
925 control of EPB technology. Tunnelling and Underground Space Technology 75, 117–128,
926 *https://doi.org/10.1016/j.tust.2018.02.006*.
927 Ochmański, M., Modoni, G. and Spagnoli, G. (2020). Influence of the annulus grout on the
928 soil-lining interaction for EBP tunneling. Proc. of 10th International Symposium on
929 Geotechnical Aspects of Underground Construction in Soft Ground (in press).
930 Oh, J.Y. and Ziegler, M. (2014). Investigation on influence of tail void grouting on the
931 surface settlements during shield tunneling using a stress-pore pressure coupled analysis.
932 KSCE Journal of Civil Engineering, 18(3), 803-811, DOI: *10.1007/s12205-014-1383-8*.
933 Oggeri C. and Ova G. (2004). Quality in tunnelling: ITA-AITES Working Group 16 Final
934 report. Tunnelling and Underground Space Technology 19,(3) 239–227,
935 doi:10.1016/j.tust.2004.01.002.
936 Oke, J., Vlachopoulos, N. and Diederichs, M. (2018). Improvement to the Convergence-
937 Confinement Method: Inclusion of Support Installation Proximity and Stiffness. Rock
938 Mechanics and Rock Engineering, 51, 1495–1519, https://doi.org/10.1007/s00603-018-
939 1418-0.
940 Oreste P. (2003). Analysis of structural interaction in tunnels using the covergence–
941 confinement approach, Tunnelling and Underground Space Technology, Volume 18, Issue
942 4, August 2003, Pages 347-363.

Oreste P. (2007). A numerical approach to the hyperstatic reaction method for the dimensioning of tunnel supports. Tunn. Undergr. Sp. Tech., 22, 185–205.

Oreste P (2009) The convergence–confinement method: roles and limits in modern geomechanical tunnel design. Am J Appl Sci 6(4):757–771.

Oreste P (2015) Analysis of the Interaction between the Lining of a TBM Tunnel and the Ground Using the Convergence-Confinement Method. American Journal of Applied Sciences 12 (4), 276-283.

Oreste, P., Spagnoli, G., and Lo Bianco, L. (2016). A Combined Analytical and Numerical Approach for the Evaluation of Radial Loads on the Lining of Vertical Shafts. Geotechnical and Geological Engineering 34 (4), 1057-1065, *https://doi.org/10.1007/s10706-016-0026-6*.

Oreste P., Spagnoli G., Luna Ramos A.C., and Sebille L. (2018a). The Hyperstatic Reaction Method for the Analysis of the Sprayed Concrete Linings Behavior in Tunneling. Geotech. Geol. Eng., 36(4), 2143–2169 https://doi.org/10.1007/s10706-018-0454-6.

Oreste P., Spagnoli G., and Luna Ramos A.C., (2018b). The Elastic Modulus Variation During the Shotcrete Curing Jointly Investigated by the Convergence-Confinement and the Hyperstatic Reaction Methods. Geotech. Geol. Eng., *https://doi.org/10.1007/s10706-018-0698-1*.

Oreste P., Spagnoli G., Luna Ramos A.C., and Hedayat, A. (2019) Assessment of the Safety Factor Evolution of the Shotcrete Lining for Different Curing Ages. Geotechnical and Geological Engineering 37 (6), 5555-5563, *https://doi.org/10.1007/s10706-019-00990-2*.

Park, H., Oh, J.Y., Kim, D., and Chang S. (2018). Monitoring and analysis of ground settlement induced by tunnelling with slurry pressure-balanced Tunnel Boring Machine. Advances in Civil Engineering, 2018, ID 5879402, *https://doi.org/10.1155/2018/5879402*.

968 Pelizza, S., Peila, D., Sorge, R., Cignitti, F. (2011). Back-fill grout with two component mix
969 in EPB tunneling to minimize surface settlements: Rome Metro - Line C case history.
970 Proceedings of Geotechnical Aspects of Underground Construction in Soft Ground,
971 Viggiani, G. (ed.), 291-299, Taylor & Francis Group, London.
972 Pelizza, S., Oreste, P.P., Peila, D., Oggeri, C. (2000), Stability analysis of a large cavern in
973 Italy for quarrying exploitation of a pink marble. Tunnelling and Underground Space
974 Technology 15(4), pp. 421-435.
975 Serafim, J. L., and Pereira, J. P. (1983). Constructions of the geomechanics classification
976 of Bieniawski. In Proc. Int. Symp. on Engg. Geol. and Underground Construction. LNEC,
977 Lisob, Portugal.
978 Shah, R., Lavasan, A.A., Peila, D., Todaro, C., Luciani, A. and Schanz, T. (2018).
979 Numerical study on backfilling the tail void using a two-component grout. J. Mater. Civ.
980 Eng., 30(3): 04018003.
981 Spagnoli, G., Oreste, P., and Lo Bianco L. (2016). New Equations for Estimating Radial
982 Loads on Deep Shaft Linings in Weak Rocks. International Journal of Geomechanics 16
983 (6), 06016006, *https://doi.org/10.1061/(ASCE)GM.1943-5622.0000657*.
984 Spagnoli, G., Oreste, P., and Lo Bianco L. (2017). Estimation of Shaft Radial
985 Displacement beyond the Excavation Bottom before Installation of Permanent Lining in
986 Nondilatant Weak Rocks with a Novel Formulation. International Journal of Geomechanics
987 17 (9), 04017051, *https://doi.org/10.1061/(ASCE)GM.1943-5622.0000949*.
988 Talmon, A.M. and Bezuijen, A. (2005). Grouting the tail void of bored tunnels: the role of
989 hardening and consolidation of grouts. Proceedings of the 5th International Symposium TC
990 28 - Geotechnical Aspects of Underground Construction in Soft Ground, 125-130,
991 Balkema, Rotterdam.
992 Thewes, M. and Budach, C. (2009). Grouting of the annular gap in shield tunnelling-An
993 important factor for minimisation of settlements and production performance. Proceedings

994 of the ITA-AITES World Tunnel Congress 2009 “Safe Tunnelling for the City and
995 Environment”, pp. 1–9.
996 Todaro, C., Peila, L., Luciani, A., Carigi, A., Martinelli, D. and Boscaro, A. (2019). Two
997 component backfilling in shield tunneling: laboratory procedure and results of a test
998 campaign. In Proceedings of the WTC 2019 ITA-AITES World Tunnel Congress (WTC
999 2019), May 3-9, 2019, Naples, Italy, Peila, D., Viggiani, G. and Celestino, T. (eds), CRC
1000 Press, Boca Raton.
1001 Vu, M.N., Broere, W. and Bosch, J. (2016). Volume loss in shallow tunnelling. Tunnelling
1002 and Underground Space, 59, 77-90, doi: 10.1016/j.tust.2016.06.011.